Journal of Computational Physics 328 (2017) 413–437

Contents lists available at ScienceDirect

Journal of Computational Physics

www.elsevier.com/locate/jcp

A free energy satisfying discontinuous Galerkin method for one-dimensional Poisson–Nernst–Planck systems

Hailiang Liu [a,*], Zhongming Wang [b]

[a] Iowa State University, Mathematics Department, Ames, IA 50011, United States
[b] Florida International University, Department of Mathematics and Statistics, Miami, FL 33199, United States

ARTICLE INFO

Article history:
Received 22 July 2016
Received in revised form 18 September 2016
Accepted 3 October 2016
Available online 24 October 2016

Keywords:
Poisson–Nernst–Planck equation
Free energy
Discontinuous Galerkin methods

ABSTRACT

We design an arbitrary-order free energy satisfying discontinuous Galerkin (DG) method for solving time-dependent Poisson–Nernst–Planck systems. Both the semi-discrete and fully discrete DG methods are shown to satisfy the corresponding discrete free energy dissipation law for positive numerical solutions. Positivity of numerical solutions is enforced by an accuracy-preserving limiter in reference to positive cell averages. Numerical examples are presented to demonstrate the high resolution of the numerical algorithm and to illustrate the proven properties of mass conservation, free energy dissipation, as well as the preservation of steady states.

1. Introduction

In this paper, we develop an arbitrary-order free energy satisfying numerical method for solving the initial boundary value problem of the Poisson–Nernst–Planck (PNP) system,

$$\partial_t c_i = \nabla \cdot (\nabla c_i + q_i c_i \nabla \psi), \quad x \in \Omega,\ t > 0, \tag{1.1a}$$

$$-\Delta \psi = \sum_{i=1}^{m} q_i c_i + \rho_0(x), \quad x \in \Omega,\ t > 0, \tag{1.1b}$$

$$c_i(0,x) = c_i^{\text{in}}(x), \quad x \in \Omega, \tag{1.1c}$$

$$\frac{\partial \psi}{\partial \mathbf{n}} = \sigma, \quad \frac{\partial c_i}{\partial \mathbf{n}} + q_i c_i \frac{\partial \psi}{\partial \mathbf{n}} = 0, \qquad x \in \partial\Omega,\ t > 0, \tag{1.1d}$$

where $c_i = c_i(t,x)$ is the local concentration of ith charged molecular or ion species with charge q_i $(1 \le i \le m)$ at the spatial point x and time t, $\Omega \subset \mathbb{R}^d$ denotes a connected closed domain with smooth boundary $\partial\Omega$, $\psi = \psi(t,x)$ is the electrostatic potential governed by the Poisson equation subject to the Neumann boundary data σ and the charge density that consists of both fixed charge ρ_0 and mobile ions, the latter being a linear combination of all the concentrations c_i. Here $\mathbf{n}$ is the unit outward normal vector on the domain boundary $\partial\Omega$. In this system, the diffusion coefficient, the thermal energy and the dielectric coefficient have been normalized in a dimensionless manner.

* Corresponding author.
E-mail addresses: hliu@iastate.edu (H. Liu), zwang6@fiu.edu (Z. Wang).

http://dx.doi.org/10.1016/j.jcp.2016.10.008
0021-9991/

The side conditions are necessarily compatible, i.e.,

$$\int_\Omega \left(\sum_{i=1}^m q_i c_i^{\text{in}}(x) + \rho_0(x)\right) dx + \int_{\partial\Omega} \sigma\, ds = 0, \tag{1.2}$$

for the solvability of the problem.

The PNP system is a mean field approximation of diffusive molecules or ions, and consists of Nernst–Planck (NP) equations that describe the drift and diffusion of ion species, and the Poisson equation that describes the electrostatics interaction. In the process of charge transport the fluxes of charge carriers are driven exclusively by processes of diffusion and electric drift. This description using the flux traces back to Nernst [44] and Planck [45], and is accurate for modeling systems with point charges. Applications of this system are found in electrical engineering and electrokinetics [17,26,28,39,40,42], electrochemistry [23], and biophysics [18,25].

Three main properties of the solution to (1.1) are the non-negativity, mass conservation and the free energy dissipation, i.e.,

$$c_i^{\text{in}}(x) \geq 0 \Longrightarrow c_i(t,x) \geq 0, \quad \forall t > 0,\ x \in \Omega, \tag{1.3a}$$

$$\int_\Omega c_i(t,x)\, dx = \int_\Omega c_i^{\text{in}}(x)\, dx, \quad \forall t > 0, \tag{1.3b}$$

$$\frac{d}{dt} F = -\sum_{i=1}^m \int_\Omega c_i^{-1} |\nabla c_i + q_i c_i \nabla \psi|^2 dx + \int_{\partial\Omega} \partial_t \sigma\, \psi\, ds, \tag{1.3c}$$

where the free energy F is defined by

$$F = \int_\Omega \sum_{i=1}^m c_i \log c_i dx + \frac{1}{2} \int_\Omega |\nabla_x \psi|^2 dx. \tag{1.4}$$

The free energy contains both entropic part and the interaction part: $c_i \log c_i$ is the entropy related to the Brownian motion of each ion species, and $\frac{1}{2}\int_\Omega |\nabla_x \psi|^2 dx$ is the electrostatic potential of the Coulomb interaction between charged ions. For the PNP system, the density is expected to converge to the equilibrium solution in a closed system (e.g. $\sigma = 0$) regardless of how initial data are distributed.

These nice mathematical features are crucial for the analytical study of the PNP system. For instance, by some energy estimate with the control of the free energy dissipation, the solution is shown to converge to the thermal equilibrium state as time becomes large, if the boundary conditions are in thermal equilibrium (see, e.g., [22]). Long time behavior was studied in [8], and further in [1,6] with refined convergence rates. Results for the drift–diffusion model regarding existence and asymptotic studies in the case of different boundary conditions may be found in [19–21].

1.1. Existing and proposed methods

Due to the wide variety of devices modeled by the PNP equations, computer simulation for this system of differential equations is of great interest. In addition to being more computationally efficient, PNP models more easily incorporate certain types of boundary conditions that arise in physical systems, such as boundaries of fixed concentration or electrostatic potential. However, the PNP equations present difficulties when computing approximate solutions: it is a strongly coupled system of $m+1$ nonlinear equations, so that computational efficiency plays a critical role in applications of a numerical solver. The transport equations are often convection-dominated, numerical simulation may produce negative ion concentrations or oscillations in the computed solution, if not properly addressed.

In the literature, there are different numerical approximations available for the steady state Poisson–Nernst–Planck equations, see e.g. [2,9,26,39,42]. Computational algorithms for time-dependent PNP systems have also been constructed for both one-dimensional and two or three-dimensional models in various chemical/biological applications, and have been combined with the Brownian Dynamics simulations. The proposed algorithms range from finite difference methods [11–13,27,41,50,51,54] to finite element methods [16,37,38,43,46]. Many of existing algorithms are introduced to handle specific settings in complex applications, in which one may encounter different numerical obstacles, such as discontinuous coefficients, singular charges, geometric singularities, and nonlinear couplings to accommodate various phenomena exhibited by biological ion channels. For a broader overview of proposed algorithms, we refer the interested reader to a recent review article [53].

Given the existing rich literature, the most distinct feature of this work is the use of properties (1.3a)–(1.3c) as a guide to design an arbitrary high order algorithm to efficiently simulate the solution at large times. The most related works to the present one are [30,31,43] and in spirit [14,15,22,34–36]. The second order finite difference method introduced in [30] satisfies all three properties in (1.3) at the discrete level. For the class of nonlinear Fokker–Planck (NFP) equations

$$\partial_t c = \nabla_x \cdot (f(c) \nabla_x (\psi(x) + H'(c))), \tag{1.5}$$

with the potential ψ given, the high order discontinuous Galerkin method introduced in [31] is shown to satisfy the discrete entropy dissipation law. If the potential ψ is governed by the Poisson equation such as (1.1b), $f(c) = c$ and $H(c) = c\log c$, then (1.5) becomes the PNP system (1.1) with single species. A finite element method to the PNP system is recently introduced in [43] using a logarithmic transformation of the charge carrier densities, while the involved energy estimate resembles the physical energy law that governs the PNP system in the continuous case. The main objective of this work is to develop a high order DG method that incorporates mathematical features (1.3) to handle the coupling of the Poisson equation and the NP system so that the numerical solution remains faithful for long time simulations.

The discontinuous Galerkin (DG) method we present here is a class of finite element methods, using a completely discontinuous piecewise polynomial space for the numerical solution and the test functions. One main advantage of the DG method is the flexibility afforded by local approximation spaces combined with the suitable design of numerical fluxes crossing cell interfaces. More general information about DG methods for elliptic, parabolic, and hyperbolic PDEs can be found in the recent books and lecture notes see, e.g. [24,47,48]. The DG discretization we use here is motivated by the direct discontinuous Galerkin (DDG) method proposed in [32,33]. The main feature in the DDG schemes lies in numerical flux choices for the solution gradient, which involve higher order derivatives evaluated across cell interfaces. The entropy satisfying methods recently developed in [30,31,34–36] are the main references for the present work.

The main results in this paper include the formulation of an arbitrary-order DG methods, proofs of the discrete free energy dissipation and mass conservation for both semi-discrete and fully discrete DG methods, and an accuracy-preserving limiter to ensure the positivity preserving property for c_i. Numerical results are in excellent agreement with the analysis.

We point out that different boundary conditions are used in applications, and they are important in driving the system out of equilibrium and produce the non-vanishing ionic fluxes. The numerical method presented in this work can be easily modified to incorporate different boundary conditions, through selection of appropriate boundary fluxes (see section 2).

1.2. Related models

The PNP system has many variants by simply altering the definition of the charge carrier flux. For example, the PNP system coupled with the Navier–Stokes equation is a basic model in the study of electrokinetics [28]. It reduces to simpler models when some of ion species become trivial or steady. For example, in the case of $m = 1$, if $c_1 = c$ with $q_1 = 1$, we have

$$\partial_t c = \nabla\cdot(\nabla c + c\nabla\psi), \quad x\in\Omega,\ t>0, \tag{1.6a}$$

$$-\Delta\psi = c + \rho_0(x), \quad x\in\Omega, t>0, \tag{1.6b}$$

$$c(0,x) = c^{\text{in}}(x), \quad x\in\Omega, \tag{1.6c}$$

$$\frac{\partial\psi}{\partial\mathbf{n}} = \sigma, \quad \frac{\partial c}{\partial\mathbf{n}} + c\frac{\partial\psi}{\partial\mathbf{n}} = 0, \quad x\in\partial\Omega,\ t>0. \tag{1.6d}$$

It may well be the case that when some species still evolve in time, the others are already at the steady states due to different time scales. For example, in the case of $m = 2$, if $c_1 = c$ and $c_2 = S(x)$ with $q_1 = 1 = -q_2$, we obtain

$$\partial_t c = \nabla\cdot(\nabla c + c\nabla\psi), \quad x\in\Omega, t>0, \tag{1.7a}$$

$$0 = \nabla\cdot(\nabla S - S\nabla\psi), \quad x\in\Omega, t>0, \tag{1.7b}$$

$$-\Delta\psi = c + \rho_0(x) + S(x), \quad x\in\Omega, t>0, \tag{1.7c}$$

$$c(0,x) = c^{\text{in}}(x), \quad x\in\Omega, \tag{1.7d}$$

$$\frac{\partial\psi}{\partial\mathbf{n}} = \sigma, \quad \frac{\partial S}{\partial\mathbf{n}} - \sigma S = 0, \quad \frac{\partial c}{\partial\mathbf{n}} + \sigma c = 0, \quad x\in\partial\Omega,\ t>0. \tag{1.7e}$$

If all ion species are at the equilibrium states $c_i = \lambda_i e^{-q_i\psi}$, with $\lambda_i = \int_\Omega c_i^{\text{in}}(x)dx\left(\int_\Omega e^{-q_i\psi}dx\right)^{-1}$ so that the total density remains as given initially, the Poisson equation thus becomes a Poisson–Boltzmann equation (PBE) of the form

$$-\Delta\psi = \sum_{i=1}^{m}\left(q_i\int_\Omega c_i^{\text{in}}(x)dx\right)\frac{e^{-q_i\psi}}{\int_\Omega e^{-q_i\psi}dx} + \rho_0(x), \quad x\in\Omega, \quad \frac{\partial\psi}{\partial\mathbf{n}}\Big|_{\partial\Omega} = 0. \tag{1.8}$$

We should point out that the numerical method presented in this paper may be used as an iterative algorithm to numerically compute the reduced system (1.7) and the nonlocal PBE (1.8), which plays essential roles in chemistry and biophysics.

In a larger context, the concentration equation also links to the general class of aggregation equations with diffusion

$$\partial_t c + \nabla\cdot(c\nabla(G*c)) = \Delta c, \tag{1.9}$$

which has been widely studied in applications such as biological swarms [4,7,52] and chemotaxis [5,10]. For chemotaxis, a wide literature exists in relation to the Keller–Segel model (see [5,10] and references therein). The left-hand-side in (1.9) represents the active transport of the density c associated to a non-local velocity field $u = \nabla(G*c)$. The potential G is usually

assumed to incorporate attractive interactions among individuals of the group, while repulsive (anti-crowding) interactions are accounted for by the diffusion in the right-hand-side. Of central role in studies of model (1.9), and also particularly relevant to the present research, is the gradient flow formulation of the equation with respect to the free energy

$$F[c] = \int_\Omega c \log c dx - \frac{1}{2}\int_\Omega \int_\Omega G(x-y)c(x)c(y)dxdy. \tag{1.10}$$

1.3. Contents

This paper is organized as follows: in Section 2, we present the DG method for the one dimensional case, and discuss how to deal with different types of boundary conditions; Section 3 is devoted to theoretical analysis for both semi-discrete and fully discrete schemes. We give the details of the numerical algorithm in Section 4, including how to compute the potential ψ_h, and the positivity preserving limiter. Numerical results are presented in Section 5. Finally, concluding remarks are given in Section 6. Further numerical implementation details are given in the appendix.

2. DG discretization in space

2.1. The DG scheme

In this section we present a DG scheme for (1.1). We consider a domain $\Omega = [a, b]$ and a mesh, which is not necessarily uniform i.e., a family of N control cells I_j such that $I_j = (x_{j-1/2}, x_{j+1/2})$ with cell center $x_j = (x_{j-1/2} + x_{j+1/2})/2$. We set

$$a = x_{1/2} < x_1 < \cdots < x_{N-1/2} < x_N < x_{N+1/2} = b,$$

and $\Delta x_j = x_{j+1/2} - x_{j-1/2}$.

Define the discontinuous finite element space

$$V_h = \{v \in L^2(\Omega), \quad v|_{I_j} \in P^k(I_j), j = 1, \cdots, N\},$$

where P^k denotes polynomials of degree at most k. We rewrite the PNP system as follows

$$\partial_t c_i = \partial_x(c_i \partial_x p_i), \ i = 1, \cdots, m, \tag{2.11a}$$

$$p_i = q_i \psi + \log c_i, \tag{2.11b}$$

$$-\partial_x^2 \psi = \sum_{i=1}^m q_i c_i + \rho_0(x), \tag{2.11c}$$

subject to initial data $c_i(0, x) = c_i^{\text{in}}(x)$, which are necessarily to meet the compatibility requirement:

$$\int_\Omega \left(\sum_{i=1}^m q_i c_i^{\text{in}}(x) + \rho_0(x)\right) dx = -\int_{\partial\Omega} \sigma ds.$$

The DG scheme is to find $c_{ih}, p_{ih}, \psi_h \in V_h$ such that for all $v_i, r_i, \eta \in V_h$, $i = 1, \cdots, m$,

$$\int_{I_j} \partial_t c_{ih} v_i dx = -\int_{I_j} c_{ih} \partial_x p_{ih} \partial_x v_i dx + \{c_{ih}\}\left(\widehat{\partial_x p_{ih}} v_i + (p_{ih} - \{p_{ih}\})\partial_x v_i\right)\Big|_{\partial I_j}, \tag{2.12a}$$

$$\int_{I_j} p_{ih} r_i dx = \int_{I_j} (q_i \psi_h + \log c_{ih}) r_i dx, \tag{2.12b}$$

$$\int_{I_j} \partial_x \psi_h \partial_x \eta dx - \left(\widehat{\partial_x \psi_h}\eta + (\psi_h - \{\psi_h\})\partial_x \eta\right)\Big|_{\partial I_j} = \int_{I_j} \left(\sum_{i=1}^m q_i c_{ih} + \rho_0\right)\eta dx, \tag{2.12c}$$

where $\widehat{\partial_x p_{ih}} = Fl(p_{ih})$ and $\widehat{\partial_x \psi_h} = Fl(\psi_h)$, with the flux operator Fl defined by

$$Fl(w) := \beta_0 \frac{[w]}{h} + \{\partial_x w\} + \beta_1 h[\partial_x^2 w]. \tag{2.13}$$

Here we have used the notation: $[q] = q^+ - q^-$, and $\{q\} = (q^+ + q^-)/2$, where q^+ and q^- are the values of q from the right and left cell interfaces, respectively. The parameters β_0 and β_1 in $Fl(w)$ are chosen to enforce the free energy satisfying property. The details of how to choose β_0 and β_1 are given and justified in Section 3.

For the ODE system (2.12), we prepare initial data c_{ih}^{in} by the projection of c_i^{in} on the discontinuous finite element space V_h so that

$$\int_{I_j} c_{ih}^{\text{in}}(x)v(x)dx = \int_{I_j} c_i^{\text{in}}(x)v(x)dx, \quad \forall v \in P^k(I_j), \quad i = 1, \cdots, m. \tag{2.14}$$

2.2. Boundary conditions

The boundary conditions are a critical component of the PNP model and determine important qualitative behavior of the solution. Various boundary conditions may be used with the PNP equations. Here we consider the simplest form of boundary conditions for the concentration and for the electric potential field. For the concentration, one usually ignores any chemical reactions at the solid boundaries and assumes a no flux condition [41,43,46], i.e.,

$$\frac{\partial c_i}{\partial \mathbf{n}} + q_i c_i \frac{\partial \psi}{\partial \mathbf{n}} = 0, \qquad x \in \partial\Omega,\ t > 0.$$

However, it should be noted that it is possible to account for reactions through, for example, using the Butler–Volmer reaction kinetics [3]. The boundary conditions for the electrostatic potential are however not unique and greatly depend on the problem under investigation. Usually, one ends up either specifying the potential or the charge density on the boundary, which corresponds to Dirichlet or Neumann boundary conditions, respectively; or using Robin boundary conditions which model capacitors at the boundary. Any combination of these boundary conditions can be applied to ψ. Therefore, at the domain boundary the numerical flux needs to be treated with care so that the pre-specified boundary conditions are properly enforced.

To incorporate the boundary condition (1.1d), we set at both $x_{1/2}$ and $x_{N+1/2}$,

$$Fl(p_{ih}) = 0,\ \{p_{ih}\} = p_{ih},\ \{c_{ih}\} = c_{ih} \quad i = 1, \cdots, m, \tag{2.15}$$

$$Fl(\psi_h) = \sigma,\ \{\psi_h\} = \psi_h. \tag{2.16}$$

For other types of boundary conditions, we only need to modify the boundary fluxes accordingly. For instance, for Dirichlet boundary conditions of the form

$$\psi(t,a) = \psi_l, \quad \psi(t,b) = \psi_r; \quad c_i(t,a) = c_{il}, \quad c_i(t,b) = c_{ir},$$

we define $\{c_{ih}\}$, $\{\psi_{ih}\}$, $Fl(\psi_{ih})$ and $Fl(p_{ih})$ at the boundary in the following way,

at $x_{1/2}$ (2.17)

$$\{c_{ih}\} = \frac{1}{2}(c_{ih}^+ + c_{il}), \quad \{\psi_h\} = \frac{1}{2}(\psi_l + \psi_h^+),$$
$$Fl(\psi_{hx}) = \beta_0(\psi_h^+ - \psi_l)/h + \psi_{hx}^+,$$
$$Fl(p_{ih}) = -\beta_0(q_i\psi_l + \log c_{il} - p_{ih}^+)/h + p_{ihx}^+,$$

at $x_{N+1/2}$ (2.18)

$$\{c_{ih}\} = \frac{1}{2}(c_{ir} + c_{ih}^-), \quad \{\psi_h\} = \frac{1}{2}(\psi_r + \psi_h^-),$$
$$Fl(\psi_{hx}) = \beta_0(\psi_r - \psi_h^-)/h + \psi_{hx}^-,$$
$$Fl(p_{ih}) = \beta_0(q_i\psi_r + \log c_{ir} - p_{ih}^-)/h + p_{ihx}^-,$$

where β_0 is the penalty parameter to be chosen.

2.3. Comments on the generalization for multidimensional case

It is straightforward to extend DG formulation (2.12) to multi-dimensional spaces. Let Ω be a convex, bounded polygonal domain in $\mathbb{R}^d$ $(d = 2, 3)$. We partition Ω into computational elements denoted by $\mathcal{T}_h = \{K\}$, and h denotes the characteristic length of all the elements of $\mathcal{T}_h$. As usual, we assume the subdivision of the domain is regular. We set the DG finite element space as

$$V_h = \{v \in L^2(\Omega) : \forall K \in \mathcal{T}_h,\ v|_K \in P^k(K)\},$$

where $P^k(K)$ is the space of polynomial functions of degree at most k on K. With such an approximation space, the semi-discrete DG scheme is to find $c_{ih}, p_{ih}, \psi_h \in V_h$ such that for all $v_i, r_i, \eta \in V_h$, $i = 1, \cdots, m$,

$$\int_K \partial_t c_{ih} v_i dx = -\int_K c_{ih} \nabla_x p_{ih} \cdot \nabla_x v_i dx + \int_{\partial K} \{c_{ih}\} \left(\widehat{\partial_n p_{ih}} v_i + (p_{ih} - \{p_{ih}\}) \partial_n v_i \right) ds, \tag{2.19a}$$

$$\int_K p_{ih} r_i dx = \int_K (q_i \psi_h + \log c_{ih}) r_i dx, \tag{2.19b}$$

$$\int_K \nabla_x \psi_h \cdot \nabla_x \eta dx - \int_{\partial K} \left(\widehat{\partial_n \psi_h} \eta + (\psi_h - \{\psi_h\}) \partial_n \eta \right) ds = \int_K \left(\sum_{i=1}^m q_i c_{ih} + \rho_0 \right) \eta dx, \tag{2.19c}$$

where $\widehat{\partial_n p_{ih}} = Fl_n(p_{ih})$ and $\widehat{\partial_n \psi_h} = Fl_n(\psi_h)$, with the flux operator Fl_n defined on the interface e by

$$Fl_n(w) := \beta_0 \frac{[w]}{h_e} + \{\partial_n w\} + \beta_1 h_e [\partial_n^2 w]. \tag{2.20}$$

Here the normal vector n is assumed to be oriented from K_1 to K_2, sharing a common edge (face) e, and h_e is the characteristic length of e. $\partial_n w$ and $\partial_n^2 w$ denote the first and second order derivative along direction n, respectively. The average $\{w\}$ and the jump $[w]$ of w on e are as follows:

$$\{w\} = \frac{1}{2}(w|_{K_1} + w|_{K_2}), \quad [w] = w|_{K_2} - w|_{K_1} \quad \forall e \in \partial K_1 \cap \partial K_2.$$

For e in the set of boundary edges, each numerical solution has a uniquely defined restriction on e, while boundary conditions can be weakly enforced through the boundary fluxes in the same way as in the one-dimensional case (see Section 2.2). Most of the one-dimensional analysis presented in this work can be easily carried over to the multi-dimensional case, as long as both the bound $\Gamma(\beta_1, 1)$ as in (3.24), and some mesh-dependent inverse inequalities such as those in Lemma 3.2 can be established. However, for this coupled nonlinear system the implementation of the multi-dimensional algorithm is much more involved, and will be left in future work.

3. Properties of the PNP system and the DG method

3.1. Properties of the continuous PNP system

Under the zero flux condition for c_i in (1.1d) and the evolution law (1.1a), the total mass for each c_i $(i = 1, \cdots, m)$ is conserved in the sense that

$$\begin{aligned} \frac{d}{dt} \int_\Omega c_i(t,x) dx &= \int_\Omega \nabla_x \cdot (\nabla c_i + q_i c_i \nabla \psi) dx \\ &= \int_{\partial\Omega} \left(\frac{\partial c_i}{\partial \mathbf{n}} + q_i c_i \frac{\partial \psi}{\partial \mathbf{n}} \right) ds \\ &= 0. \end{aligned}$$

Furthermore, assume the Dirichlet boundary condition is given and homogeneous, then the stability of the solution to the PNP system is known [6,8] to be given by the energy law of the form

$$\frac{d}{dt} \left\{ \int_\Omega \sum_{i=1}^m c_i(\log c_i - 1) + \frac{1}{2} |\nabla_x \psi|^2 dx \right\} = -\int_\Omega \sum_{i=1}^m c_i |\nabla_x (\log c_i + q_i \psi)|^2 dx,$$

where the functional,

$$\int_\Omega \sum_{i=1}^m c_i(\log c_i - 1) + \frac{1}{2} |\nabla_x \psi|^2 dx$$

is the energy and

$$\int_\Omega \sum_{i=1}^m c_i |\nabla_x (\log c_i + q_i \psi)|^2 dx \geq 0$$

is the rate of dissipation. For the Neumann boundary conditions, we show the corresponding energy law by a formal calculation. First, the free energy (1.4) by the Poisson equation can be rewritten as

$$F = F_1 + F_2 := \sum_{i=1}^{m} \int_\Omega c_i \log c_i dx + \frac{1}{2} \int_\Omega |\nabla_x \psi|^2 dx.$$

We formally calculate the change rate of each part of the free energy

$$\begin{aligned}
\frac{d}{dt} F_1(t) &= \sum_{i=1}^{m} \int_\Omega (1 + \log c_i) \partial_t c_i dx \\
&= -\sum_{i=1}^{m} \int_\Omega \nabla_x (\log c_i) \cdot (\nabla_x c_i + q_i c_i \nabla_x \psi) dx \\
&= -\sum_{i=1}^{m} \int_\Omega \left(c_i^{-1} |\nabla_x c_i|^2 + q_i \nabla_x c_i \cdot \nabla_x \psi \right) dx
\end{aligned}$$

and

$$\begin{aligned}
\frac{d}{dt} F_2(t) &= \int_\Omega \nabla_x \psi \cdot \partial_t (\nabla_x \psi) dx \\
&= \int_{\partial\Omega} \psi \, \partial_t (\partial_n \psi) ds + \int_\Omega \psi \, \partial_t (-\Delta \psi) dx \\
&= \int_{\partial\Omega} \psi \, \partial_t \sigma \, ds + \sum_{i=1}^{m} \int_\Omega \psi (q_i \partial_t c_i) dx \\
&= \int_{\partial\Omega} \psi \, \partial_t \sigma \, ds - \sum_{i=1}^{m} \int_\Omega \nabla_x (q_i \psi) \cdot (\nabla_x c_i + q_i c_i \nabla_x \psi) dx \\
&= \int_{\partial\Omega} \psi \, \partial_t \sigma \, ds - \sum_{i=1}^{m} \int_\Omega q_i \nabla_x \psi \cdot \nabla_x c_i dx - \sum_{i=1}^{m} \int_\Omega q_i^2 c_i |\nabla_x \psi|^2 dx.
\end{aligned}$$

Putting together we obtain

$$\frac{d}{dt} F = \int_{\partial\Omega} \psi \, \partial_t \sigma \, ds - \sum_{i=1}^{m} \int_\Omega c_i^{-1} |\nabla_x c_i + q_i c_i \nabla_x \psi|^2 dx.$$

For the case of $\partial_t \sigma = 0$ we have

$$\frac{d}{dt} F = -\sum_{i=1}^{m} \int_\Omega c_i^{-1} |\nabla_x c_i + q_i c_i \nabla_x \psi|^2 dx \le 0.$$

Remark 3.1. In the special case that $\sigma = 0$ and $\rho_0 = 0$, both F_1 and F_2 are each decreasing in time, with

$$\begin{aligned}
\frac{d}{dt} F_1 &= -\int_\Omega \sum_{i=1}^{m} c_i^{-1} |\nabla_x c_i|^2 dx - \int_\Omega |\Delta \psi|^2 dx \le 0, \\
\frac{d}{dt} F_2 &= -\int_\Omega \left(\sum_{i=1}^{m} q_i^2 c_i \right) |\nabla_x \psi|^2 dx - \int_\Omega |\Delta \psi|^2 dx \le 0.
\end{aligned}$$

This can be verified by a direct calculation as

$$\begin{aligned}
-\sum_{i=1}^{m} \int_\Omega q_i \nabla_x \psi \cdot \nabla_x c_i dx &= \int_\Omega (\Delta \psi) \sum_{i=1}^{m} (q_i c_i) dx - \int_{\partial\Omega} \sigma \sum_{i=1}^{m} (q_i c_i) ds \\
&= -\int_\Omega |\Delta \psi|^2 dx.
\end{aligned}$$

3.2. Properties of the semi-discrete DG method

For some $M(x) > 0$, we define the weighted bilinear operator

$$A_M(u, v) = \sum_{j=1}^{N} \int_{I_j} M\partial_x u \partial_x v dx + \sum_{j=1}^{N-1} \left(\{M\}(\widehat{u_x}[v] + \{v_x\}[u])\right)_{j+1/2},$$

and the associated energy norm

$$\|v\|_{M,E}^2 = \sum_{j=1}^{N} \int_{I_j} M v_x^2 dx + \sum_{j=1}^{N-1} \frac{\beta_0}{h} \left(\{M\}[v]^2\right)_{j+1/2}.$$

When $M = 1$, we denote $\|v\|_{1,E} = \|v\|_E$. We also introduce the notation,

$$\Gamma(\beta_1, M) := \sup_{u \in P^{(k-1)}([-1,1])} \frac{2(u(1) - 2\beta_1 \partial_\xi u(1))^2}{\int_{-1}^{1} w_j(\xi) u^2(\xi) d\xi} \tag{3.21}$$

with

$$w_j(\xi) = \min\left\{M(x_j + \frac{h}{2}\xi), M(x_{j+1} - \frac{h}{2}\xi)\right\}.$$

We recall the following estimates.

Lemma 3.1. *(Cf. [35].) If $\beta_0 > \Gamma(\beta_1, M)\{M\}$ at each interface $x_{j+1/2}$, $j = 1, \cdots, N-1$, then*

$$A_M(v, v) \geq \gamma \|v\|_{M,E}^2 + \frac{1}{2} \int_{I_1 \cup I_N} M v_x^2 dx \tag{3.22}$$

for some $\gamma \in (0, 1)$. We also have

$$\Gamma(\beta_1, M) \geq \frac{2h([\partial_x w] + \beta_1 h[\partial_x^2 w])^2}{\left(\int_{I_j} + \int_{I_{j+1}}\right) M(\partial_x w)^2 dx}, \forall w \in V_h. \tag{3.23}$$

Remark 3.2. The additional terms $\frac{1}{2}\int_{I_1 \cup I_N} M v_x^2 dx$ were not used in [35]; here we need them to control boundary contributions.

In the case of $M = 1$, the bound $\Gamma(\beta_0, 1)$ is obtained in [29]:

$$\Gamma(\beta_1, 1) = k^2 \left(1 - \beta_1(k^2 - 1) + \frac{\beta_1^2}{3}(k^2 - 1)^2\right), \tag{3.24}$$

which achieves its minimum $k^2/4$ at $\beta_1 = \frac{3}{2(k^2-1)}$.

We first examine the existence and uniqueness of ψ_h from solving (2.12c). Note that for Neumann boundary data, only σ_a and σ_b are pre-specified so that

$$\sigma_a - \sigma_b = \int_a^b \rho(t, x) dx, \quad \rho(t, x) = \rho_0(x) + \sum_{i=1}^{m} q_i c_i(t, x),$$

yet $\psi(t, a)$ and $\psi(t, b)$ are not given, the exact solution is unique up to an additive constant.

Theorem 3.1. *Assume that $\beta_0 > \Gamma(\beta_1, 1)$, then for each given ρ, there exists a unique ψ_h to (2.12c) with (2.13) and (2.16), up to an additive constant.*

Proof. It suffices to prove the uniqueness since existence is implied by uniqueness for this finite dimensional problem. Let $\eta = \psi_{h1} - \psi_{h2}$ for two different solutions ψ_{hi}, then

$$A_1(\eta, \eta) = 0.$$

On the other hand, Lemma 3.1 ensures that there exists $\gamma \in (0,1)$ such that

$$A_1(\eta,\eta) \geq \gamma \|\eta\|_E^2 = \gamma \left(\sum_{j=1}^{N} \int_{I_j} \eta_x^2 dx + \sum_{j=1}^{N-1} \frac{\beta_0}{h} [\eta]_{j+1/2}^2 \right).$$

Hence η must be a constant. □

We next prove the conservation of c_{ih} and the semi-discrete free energy dissipation law.

Theorem 3.2.

1. *The semi-discrete scheme is conservative in the sense that each total concentration c_{ih} $(i = 1, \cdots, m)$ remains unchanged in time,*

$$\frac{d}{dt} \sum_{j=1}^{N} \int_{I_j} c_{ih}(t,x) dx = 0, \quad t > 0. \tag{3.25}$$

2. *Suppose that $\partial_t \sigma = 0$ and $c_{ih}(t,x) > 0$ in each I_j, the semi-discrete free energy*

$$F = \sum_{j=1}^{N} \int_{I_j} \left[\sum_{i=1}^{m} c_{ih} \log c_{ih} + \frac{1}{2} \left(\sum_{i=1}^{m} q_i c_{ih} + \rho_0 \right) \psi_h \right] dx + \frac{1}{2} \int_{\partial\Omega} \sigma \psi_h ds$$

satisfies

$$\frac{d}{dt} F = - \sum_{i=1}^{m} A_{c_{ih}}(p_{ih}, p_{ih}). \tag{3.26}$$

Moreover,

$$\frac{d}{dt} F \leq 0,$$

provided β_0 is suitably large, and $\beta_1 = 0$ in $Fl(\psi_h)$ defined in (2.13) and (2.16).

Proof. 1. The conservation (3.25) follows from taking $v_i = 1$ in (2.12a) with summation over j.

2. Set

$$\rho_h(t,x) = \sum_{i=1}^{m} q_i c_{ih}(t,x) + \rho_0(x).$$

A direct calculation using $\sum_{j=1}^{N} \int_{I_j} \partial_t c_{ih} dx = 0$ and the assumption of $\sigma_t = 0$ gives

$$\begin{aligned} \frac{d}{dt} F &= \sum_{j=1}^{N} \int_{I_j} \sum_{i=1}^{m} (1 + \ln c_{ih} + q_i \psi_h) \partial_t c_{ih} dx + \frac{1}{2} \sum_{j=1}^{N} \int_{I_j} [\rho_h \partial_t \psi_h - \partial_t \rho_h \psi_h] dx + \frac{1}{2} \int_{\partial\Omega} \sigma \partial_t \psi_h ds \\ &= \sum_{j=1}^{N} \int_{I_j} \sum_{i=1}^{m} (\ln c_{ih} + q_i \psi_h) \partial_t c_{ih} dx + \frac{1}{2} \sum_{j=1}^{N} \int_{I_j} [\rho_h \partial_t \psi_h - \partial_t \rho_h \psi_h] dx + \frac{1}{2} \int_{\partial\Omega} \sigma \partial_t \psi_h ds. \end{aligned}$$

From (2.12b) with $r_i = \partial_t c_{ih}$ it follows that

$$\int_{I_j} (\ln c_{ih} + q_i \psi_h) \partial_t c_{ih} dx = \int_{I_j} p_{ih} \partial_t c_{ih} dx.$$

Summing (2.12a) in i, j with $v_i = p_{ih}$ gives

$$\sum_{j=1}^{N} \int_{I_j} \sum_{i=1}^{m} \partial_t c_{ih} p_{ih} dx = - \sum_{j=1}^{N} \int_{I_j} \sum_{i=1}^{m} c_{ih} |p_{ihx}|^2 dx - \sum_{j=1}^{N-1} \sum_{i=1}^{m} (\{c_{ih}\}[p_{ih}](\widehat{p_{ihx}} + \{p_{ihx}\}))_{j+1/2},$$

since $\widehat{p}_{hx,\frac{1}{2}} = \widehat{p}_{hx,N+\frac{1}{2}} = 0$. Next we sum (2.12c) over all cell index j to obtain

$$A_1(\psi_h, \eta) = \sum_{j=1}^{N} \int_{I_j} \rho_h \eta dx + \int_{\partial\Omega} \sigma \eta ds. \tag{3.27}$$

In one dimensional case,

$$\int_{\partial\Omega} \sigma \eta ds = \sigma_b \eta^-_{N+1/2} - \sigma_a \eta^+_{1/2}.$$

Taking derivative of (3.27) with respect to t we also have

$$A_1(\partial_t \psi_h, \eta) = \sum_{j=1}^{N} \int_{I_j} \partial_t \rho_h \eta dx. \tag{3.28}$$

Thus (3.27) with $\eta = \partial_t \psi_h$ subtracted by (3.28) with $\eta = \psi_h$ gives

$$\begin{aligned}\sum_{j=1}^{N} \int_{I_j} [\rho_h \partial_t \psi_h - \partial_t \rho_h \psi_h] dx + \int_{\partial\Omega} \sigma \partial_t \psi_h ds &= A_1(\psi_h, \partial_t \psi_h) - A_1(\partial_t \psi_h, \psi_h) \\ &= \beta_1 h \sum_{j=1}^{N-1} ([\partial_x^2 \psi_h][\partial_t \psi_h] - [\partial_x^2 \partial_t \psi_h][\psi_h])_{j+1/2} \\ &= 0\end{aligned}$$

since $\beta_1 = 0$ in the numerical flux $Fl(\psi_h)$ defined in (2.13).

Putting all together we obtain

$$\begin{aligned}\frac{d}{dt} F &= -\sum_{j=1}^{N} \int_{I_j} \sum_{i=1}^{m} c_{ih} |p_{ihx}|^2 dx - \sum_{j=1}^{N-1} \sum_{i=1}^{m} (\{c_{ih}\}[p_{ih}](\widehat{p_{ihx}} + \{p_{ihx}\}))_{j+1/2} \\ &= -\sum_{i=1}^{m} A_{c_{ih}}(p_{ih}, p_{ih}) \\ &\le 0,\end{aligned}$$

if at each interface $\beta_0 > \max_i \Gamma(\beta_1, c_{ih})\{c_{ih}\}$, as shown in Lemma 3.1.

Remark 3.3. For (β_0, β_1) in the numerical flux formulation (2.13), we use $\beta_0 > k^2$ and $\beta_1 = 0$ for $Fl(\psi_h)$. For $Fl(p_h)$ we need to pick

$$\beta_0 > \Gamma(\beta_1, c_{ih})\{c_{ih}\}$$

for numerical solutions c_{ih}. For sufficiently small h, variation of c_{ih} near each interface is relatively bounded by a factor 2, hence it suffices to choose

$$\beta_0 > 2\Gamma(\beta_1, 1) = 2k^2 \left(1 - \beta_1(k^2 - 1) + \frac{\beta_1^2}{3}(k^2 - 1)^2\right),$$

where (3.24) has been used. For $k > 1$, one choice is $\beta_1 = \frac{3}{2(k^2-1)}$ so that $\beta_0 > 2\Gamma(\beta_1, 1) = k^2/2$. Therefore it suffices to take $\beta_0 > k^2$ in (2.13) for both $Fl(\psi_h)$ and $Fl(p_h)$. The choices of (β_0, β_1) in our numerical simulation all fall within the range $\beta_0 > k^2$. □

3.3. Properties of the fully discrete DG method

In order to preserve the free energy dissipation law at each time step, the time step restriction is needed when using an explicit time discretization. We now discuss this issue by taking the Euler first order time discretization of (2.12) with uniform time step Δt: find $c_{ih}^{n+1}, \psi_h^{n+1} \in V_h$ such that for any $v_i, r_i, \eta \in V_h$,

$$\int_{I_j} D_t c_{ih}^n v_i dx = -\int_{I_j} c_{ih}^n \partial_x p_{ih}^n \partial_x v_i dx + \{c_{ih}^n\}\left(\widehat{\partial_x p_{ih}^n} v_i + (p_{ih}^n - \{p_{ih}^n\})\partial_x v_i\right)\Big|_{\partial I_j}, \tag{3.29a}$$

$$\int_{I_j} p_{ih}^n r_i dx = \int_{I_j} (q_i \psi_h^n + \log c_{ih}^n) r_i dx, \tag{3.29b}$$

$$\int_{I_j} \partial_x \psi_h^n \partial_x \eta dx - \left(\widehat{\partial_x \psi_h^n}\eta + (\psi_h^n - \{\psi_h^n\})\partial_x \eta\right)\Big|_{\partial I_j} = \int_{I_j}\left[\sum_{i=1}^m q_i c_{ih}^n + \rho_0\right]\eta dx. \tag{3.29c}$$

Here and in what follows, we use the notation for any function $w^n(x)$ as

$$D_t w^n = \frac{w^{n+1} - w^n}{\Delta t}.$$

We recall some basic estimates:

Lemma 3.2. *(Cf. [31, Lemma 3.2].) The following inequalities hold for any $v \in V_h$:*

$$\sum_{j=1}^N \int_{I_j} v_x^2 dx \le \frac{k(k+1)^2(k+2)}{h^2} \sum_{j=1}^N \int_{I_j} v^2 dx, \tag{3.30a}$$

$$\sum_{j=1}^{N-1} [v]_{j+1/2}^2 \le \frac{4(k+1)^2}{h} \sum_{j=1}^N \int_{I_j} v^2 dx, \tag{3.30b}$$

$$\sum_{j=1}^{N-1} \{v_x\}_{j+1/2}^2 \le \frac{k^3(k+1)^2(k+2)}{h^3} \sum_{j=1}^N \int_{I_j} v^2 dx. \tag{3.30c}$$

Based on these estimates we show several properties of the fully discret scheme (3.29).

Theorem 3.3.

1. *The fully discrete scheme (3.29) is conservative in the sense that each total concentration $c_{ih}^n(x)$ $(i = 1, \cdots, m)$ remains unchanged at each time step,*

$$\sum_{j=1}^N \int_{I_j} c_{ih}^n dx = \sum_{j=1}^N \int_{I_j} c_{ih}^{n+1} dx, \quad i = 1, \cdots, m. \tag{3.31}$$

2. *Assume that $c_{ih}^n(x) > 0$ in each I_j. There exists $\mu^* > 0$ such that if the mesh ratio $\mu = \frac{\Delta t}{\Delta x^2} \in (0, \mu^*)$, then the fully discrete free energy*

$$F^n = \sum_{j=1}^N \int_{I_j} \left[\sum_{i=1}^m c_{ih}^n \log c_{ih}^n + \frac{1}{2}\left(\sum_{i=1}^m q_i c_{ih}^n + \rho_0\right)\psi_h^n\right] dx + \frac{1}{2}\int_{\partial\Omega} \sigma \psi_h^n ds$$

satisfies

$$D_t F^n \le -\frac{1}{2}\sum_{i=1}^m A_{c_{ih}^n}(p_{ih}^n, p_{ih}^n). \tag{3.32}$$

Moreover,

$$F^{n+1} \le F^n, \tag{3.33}$$

provided that β_0 is suitably large, and $\beta_1 = 0$ in $Fl(\psi_h)$ defined in (2.13) and (2.16).

Proof. Set

$$\rho_h^n = \sum_{i=1}^m q_i c_{ih}^n + \rho_0,$$

and sum over j in (3.29) to obtain

$$\int_\Omega D_t c_{ih}^n v_i dx = -A_{c_{ih}^n}(p_{ih}^n, v_i), \tag{3.34a}$$

$$\int_\Omega p_{ih}^n r_i dx = \int_\Omega (q_i \psi_h^n + \log c_{ih}^n) r_i dx, \tag{3.34b}$$

$$A_1(\psi_h^n, \eta) = \int_\Omega \rho_h^n \eta dx + \int_{\partial\Omega} \sigma \eta ds. \tag{3.34c}$$

1. Taking $v_i = 1$ in (3.34a) yields (3.31).
2. Taking $v_i = p_{ih}^n$ in (3.34a), and $r_i = D_t c_{ih}^n$ in (3.34b), respectively, and summing over m, we obtain

$$\int_\Omega \sum_{i=1}^m (D_t c_{ih}^n) p_{ih}^n dx = -\sum_{i=1}^m A_{c_{ih}^n}(p_{ih}^n, p_{ih}^n)$$

and

$$\int_\Omega \sum_{i=1}^m p_{ih}^n (D_t c_{ih}^n) dx = \int_\Omega \sum_{i=1}^m (q_i \psi_h^n + \log c_{ih}^n) D_t c_{ih}^n dx.$$

From (3.34c) we see that

$$A_1(\psi_h^{n+1} - \psi_h^n, \eta) = \int_\Omega (\rho_h^{n+1} - \rho_h^n) \eta dx. \tag{3.35}$$

This with $\eta = \psi_h^n$ and $\rho_h^n = \sum_{i=1}^m q_i c_{ih}^n + \rho_0(x)$ yields

$$\int_\Omega \sum_{i=1}^m q_i \psi_h^n (c_{ih}^{n+1} - c_{ih}^n) dx = \int_\Omega (\rho_h^{n+1} - \rho_h^n) \psi_h^n dx = A_1(\psi_h^{n+1} - \psi_h^n, \psi_h^n). \tag{3.36}$$

These relations lead to

$$\int_\Omega \sum_{i=1}^m \log c_{ih}^n (c_{ih}^{n+1} - c_{ih}^n) dx = -\Delta t \sum_{i=1}^m A_{c_{ih}^n}(p_{ih}^n - p_{ih}^n) - A_1(\psi_h^{n+1} - \psi_h^n, \psi_h^n). \tag{3.37}$$

Note that (3.34c) with $\eta = \psi_h^{n+1} - \psi_h^n$ subtracted by (3.35) with $\eta = \psi_h^n$ gives

$$\begin{aligned} &\int_\Omega [\rho_h^n (\psi_h^{n+1} - \psi_h^n) - (\rho_h^{n+1} - \rho^n) \psi_h^n] dx + \int_{\partial\Omega} \sigma (\psi_h^{n+1} - \psi_h^n) ds \\ &\quad = A_1(\psi_h^n, \psi_h^{n+1} - \psi_h^n) - A_1(\psi_h^{n+1} - \psi_h^n, \psi_h^n) = 0. \end{aligned}$$

Also taking $\eta = \psi_h^{n+1} + \psi_h^n$ in (3.35) we obtain

$$\int_\Omega (\rho_h^{n+1} - \rho_h^n)(\psi_h^{n+1} + \psi_h^n) dx = A_1(\psi_h^{n+1} - \psi_h^n, \psi_h^{n+1} + \psi_h^n).$$

Adding these up leads to

$$\int_{\partial\Omega} \sigma (\psi_h^{n+1} - \psi_h^n) ds + \int_\Omega (\rho_h^{n+1} \psi_h^{n+1} - \rho_h^n \psi_h^n) dx = A_1(\psi_h^{n+1} - \psi_h^n, \psi_h^{n+1} + \psi_h^n). \tag{3.38}$$

With (3.37) and (3.38) we proceed to evaluate

$$\begin{aligned} F^{n+1} - F^n = &\sum_{i=1}^m \int_\Omega \left[c_{ih}^{n+1} \log c_{ih}^{n+1} - c_{ih}^n \log c_{ih}^n \right] dx + \frac{1}{2} \int_{\partial\Omega} \sigma (\psi_h^{n+1} - \psi_h^n) ds \\ &+ \frac{1}{2} \int_\Omega (\rho_h^{n+1} \psi_h^{n+1} - \rho_h^n \psi_h^n) dx \end{aligned}$$

$$
\begin{aligned}
&= \sum_{i=1}^{m} \int_{\Omega} \log c_{ih}^{n} (c_{ih}^{n+1} - c_{ih}^{n}) dx + \sum_{i=1}^{m} \int_{\Omega} c_{ih}^{n+1} \log \left(\frac{c_{ih}^{n+1}}{c_{ih}^{n}} \right) dx \\
&\quad + \frac{1}{2} A_1(\psi_h^{n+1} - \psi_h^n, \psi_h^{n+1} + \psi_h^n) \\
&= -\Delta t \sum_{i=1}^{m} A_{c_{ih}^n}(p_{ih}^n, p_{ih}^n) + \sum_{i=1}^{m} \int_{\Omega} c_{ih}^{n+1} \log \left(\frac{c_{ih}^{n+1}}{c_{ih}^{n}} \right) dx + \frac{1}{2} A_1(\psi_h^{n+1} - \psi_h^n, \psi_h^{n+1} - \psi_h^n) \\
&= -\Delta t \sum_{i=1}^{m} A_{c_{ih}^n}(p_{ih}^n, p_{ih}^n) + \sum_{i=1}^{m} \int_{\Omega} c_{ih}^{n} \log \left(\frac{c_{ih}^{n+1}}{c_{ih}^{n}} \right) dx + G^n \\
&\le -\Delta t \sum_{i=1}^{m} A_{c_{ih}^n}(p_{ih}^n, p_{ih}^n) + G^n,
\end{aligned}
$$

where the non-positivity of the second term is based on $\log X \le X - 1$ and the conservation of $\sum_{i=1}^{m} \int_{\Omega} c_{ih}^{n} dx$. Here

$$
G^n = \sum_{i=1}^{m} \int_{\Omega} (c_{ih}^{n+1} - c_{ih}^{n}) \log \left(\frac{c_{ih}^{n+1}}{c_{ih}^{n}} \right) dx + \frac{1}{2} A_1(\psi_h^{n+1} - \psi_h^n, \psi_h^{n+1} - \psi_h^n) =: G_1^n + G_2^n,
$$

which is non-negative, yet small.

It remains to figure out a sufficient restriction on the mesh ratio $\mu = \Delta t/(\Delta x)^2$ so that

$$
G^n \le \frac{\Delta t}{2} \sum_{i=1}^{m} A_{c_{ih}^n}(p_{ih}^n, p_{ih}^n). \tag{3.39}
$$

In (3.34a), we take $v_i = D_t c_{ih}^n$ and use the Young inequality $ab \le \frac{1}{4\epsilon} a^2 + \epsilon b^2$ to obtain

$$
\begin{aligned}
\sum_{j=1}^{N} \int_{I_j} v_i^2 \, dx &= -\sum_{j=1}^{N} \int_{I_j} c_{ih}^n \partial_x p_{ih}^n \partial_x v_i \, dx - \sum_{j=1}^{N-1} \{c_{ih}^n\} \left(\widehat{\partial_x p_{ih}^n} [v_i] + \{\partial_x v_i\} [p_{ih}^n] \right) \Big|_{x_{j+\frac{1}{2}}} \\
&\le \frac{1}{4\epsilon_1 h^2} \sum_{j=1}^{N} \int_{I_j} (c_{ih}^n)^2 |\partial_x p_{ih}^n|^2 \, dx + \epsilon_1 h^2 \sum_{j=1}^{N} \int_{I_j} |\partial_x v_i|^2 \, dx \\
&\quad + \frac{1}{4\epsilon_2 h} \sum_{j=1}^{N-1} \{c_{ih}^n\}^2 |\widehat{\partial_x p_{ih}^n}|^2 \Big|_{x_{j+\frac{1}{2}}} + \epsilon_2 h \sum_{j=1}^{N-1} [v_i]^2 \Big|_{x_{j+\frac{1}{2}}} \\
&\quad + \frac{1}{4\epsilon_3 h^3} \sum_{j=1}^{N-1} \{c_{ih}^n\}^2 [p_{ih}^n]^2 \Big|_{x_{j+\frac{1}{2}}} + \epsilon_3 h^3 \sum_{j=1}^{N-1} \{\partial_x v_i\}^2 \Big|_{x_{j+\frac{1}{2}}}.
\end{aligned}
$$

The use of inequalities (3.30) in Lemma 3.2 leads to

$$
\begin{aligned}
&\epsilon_1 h^2 \sum_{j=1}^{N} \int_{I_j} |\partial_x v_i|^2 \, dx + \epsilon_2 h \sum_{j=1}^{N-1} [v_i]^2 \Big|_{x_{j+\frac{1}{2}}} + \epsilon_3 h^3 \sum_{j=1}^{N-1} [\partial_x v_i]^2 \Big|_{x_{j+\frac{1}{2}}} \\
&\le (k+1)^2 (k(k+2)\epsilon_1 + 4\epsilon_2 + k^3(k+2)\epsilon_3) \sum_{j=1}^{N} \int_{I_j} v_i^2 \, dx \\
&= \frac{3}{4} \sum_{j=1}^{N} \int_{I_j} v_i^2 \, dx,
\end{aligned}
$$

if we choose ϵ_i as

$$
(4\epsilon_1)^{-1} = k(k+1)^2(k+2), \ (4\epsilon_2)^{-1} = 4(k+1)^2, \quad (4\epsilon_3)^{-1} = k^3(k+1)^2(k+2).
$$

This gives

$$\frac{1}{4}\sum_{j=1}^{N}\int_{I_j} v_i^2\,dx \le \frac{k(k+1)^2(k+2)}{h^2}\sum_{j=1}^{N}\int_{I_j}(c_{ih}^n)^2|\partial_x p_{ih}^n|^2\,dx \tag{3.40}$$
$$+\frac{k^3(k+1)^2(k+2)}{h^3}\sum_{j=1}^{N-1}\{(c_{ih}^n)\}^2[p_{ih}^n]^2\Big|_{x_{j+\frac12}}+\frac{4(k+1)^2}{h}\sum_{j=1}^{N-1}\{c_{ih}^n\}^2|\widehat{\partial_x p_{ih}^n}|^2\Big|_{x_{j+\frac12}}.$$

It is clear that the first two terms are bounded by $h^{-2}\|c_{ih}^n(\cdot)\|_\infty\|p_{ih}^n\|_{c_{ih}^n,E}^2$. We next show that the last term is also bounded by $h^{-2}\|c_{ih}^n(\cdot)\|_\infty\|p_{ih}^n\|_{c_{ih}^n,E}^2$, up to a constant multiplication factor. Note that

$$|\widehat{\partial_x p_{ih}^n}|^2\big|_{x_{j+\frac12}} = \left|\{\partial_x p_{ih}^n\}+\beta_0\frac{[p_{ih}^n]}{h}+\beta_1 h[\partial_x^2 p_{ih}^n]\right|^2$$
$$\le 2\left(\beta_0^2\frac{[p_{ih}^n]^2}{h^2}+\left(\{\partial_x p_{ih}^n\}+\beta_1 h[\partial_x^2 p_{ih}^n]\right)^2\right).$$

From (3.23) it follows that

$$\left(\{\partial_x p_{ih}^n\}+\beta_1 h[\partial_x^2 p_{ih}^n]\right)^2\Big|_{x_{j+\frac12}} \le \frac{\Gamma(\beta_1,c_{ih}^n)}{2h}\left(\int_{I_j}+\int_{I_{j+1}}\right)c_{ih}^n|\partial_x p_{ih}|^2dx.$$

Hence

$$\sum_{j=1}^{N-1}\{c_{ih}^n\}^2|\widehat{\partial_x p_{ih}^n}|^2\Big|_{x_{j+\frac12}} \le \frac{2}{h}\max\{\beta_0,\Gamma(\beta_1,c_{ih}^n)\{c_{ih}^n\}\}\|c_{ih}^n(\cdot)\|_\infty\|p_{ih}^n\|_{c_{ih}^n,E}^2$$
$$=\frac{2\beta_0}{h}\|c_{ih}^n(\cdot)\|_\infty\|p_{ih}^n\|_{c_{ih}^n,E}^2.$$

Upon insertion into (3.40) we obtain

$$\sum_{j=1}^{N}\int_{I_j} v_i^2\,dx \le \frac{C(k,\beta_0)||c_{ih}^n(\cdot)||_\infty}{h^2}\|p_{ih}^n\|_{c_{ih}^n,E}^2,$$

where

$$C(k,\beta_0) := 4(k+1)^2\left(k(k+2)\max\{1,k^2/\beta_0\}+8\beta_0\right). \tag{3.41}$$

Note that

$$G_1^n \le \sum_{i=1}^{m}\int_\Omega\frac{(c_{ih}^{n+1}-c_{ih}^n)^2}{c_{ih}^n}dx=\sum_{i=1}^{m}\int_\Omega\frac{v_i^2}{c_{ih}^n}dx(\Delta t)^2$$
$$\le\mu\Delta t\frac{C(k,\beta_0)||c_{ih}^n(\cdot)||_\infty}{\min_{i,x}c_{ih}^n}\sum_{i=1}^{m}\|p_{ih}^n\|_{c_{ih}^n,E}^2$$
$$\le\mu\Delta t\frac{C(k,\beta_0)||c_{ih}^n(\cdot)||_\infty}{\gamma\min_{i,x}c_{ih}^n}\sum_{i=1}^{m}A_{c_{ih}^n}(p_{ih}^n,p_{ih}^n)$$
$$\le\frac{\Delta t}{4}\sum_{i=1}^{m}A_{c_{ih}^n}(p_{ih}^n,p_{ih}^n),$$

if the mesh ratio satisfies

$$\mu\le\frac{\gamma\min_{i,x}c_{ih}^n}{4C(k,\beta_0)\max_i||c_{ih}^n(\cdot)||_\infty}.$$

It remains to bound G_2^n. From (3.35) it follows that for $\xi := \psi_h^{n+1}-\psi_h^n$,

$$A_1(\xi,\xi)=\sum_{i=1}^{m} q_i \int_\Omega (c_{ih}^{n+1}-c_{ih}^n)\xi dx=\Delta t\sum_{i=1}^{m} q_i \int_\Omega v_i\xi dx\le \Delta t\sum_{i=1}^{m}|q_i|\|v_i\|\|\xi\|. \tag{3.42}$$

Note that $A_1(\cdot,\cdot)$ is a symmetric bilinear operator (since $\beta_1=0$ in (2.13) for ψ_h), and also that $A_1(\xi,\xi)=0$ if and only if $\xi\equiv const$, therefore

$$c=\inf_{\{\xi\in V_h,\xi\neq \text{const}\}}\frac{h^2A_1(\xi,\xi)}{\|\xi\|^2}$$

is positive. A simple rescaling suggests that c is also independent of h. Hence $\|\xi\|^2\le c^{-1}h^2A_1(\xi,\xi)$, which when inserted into (3.42), set $C_1=\sum_{i=1}^m q_i^2/c$, leads to

$$\begin{aligned}A_1(\xi,\xi)&\le C_1(\Delta t)^2h^2\sum_{i=1}^{m}\|v_i\|^2\le C_1C(k,\beta_0)\max_i||c_{ih}^n(\cdot)||_\infty(\Delta t)^2\sum_{i=1}^{m}\|p_{ih}^n\|^2_{c_{ih}^n,E}\\&\le C_1(\Delta t)^2\frac{C(k,\beta_0)\max_i||c_{ih}^n(\cdot)||_\infty}{\gamma}\sum_{i=1}^{m}A_{c_{ih}^n}(p_{ih}^n,p_{ih}^n)\\&\le\frac{\Delta t}{4}\sum_{i=1}^{m}A_{c_{ih}^n}(p_{ih}^n,p_{ih}^n),\end{aligned}$$

as long as the time step also satisfies

$$\Delta t\le\frac{\gamma}{4C_1C(k,\beta_0)\max_i||c_{ih}^n(\cdot)||_\infty}.$$

Collecting the above estimates on G_i^n $(i=1,2)$ we obtain (3.39), if we take

$$\mu^*=\frac{\gamma}{4C(k,\beta_0)\max_i||c_{ih}^n(\cdot)||_\infty}\min\{C_1^{-1}h^{-2},\min_{i,x}c_{ih}^n\}.$$

This ends the proof. □

Remark 3.4. In Theorem 3.3, $c_{ih}(x)$ is assumed to be positive in each cell I_j to make $p_{ih}=q_i\psi_h+\log c_{ih}$ well defined. In numerical simulations, we enforce this by imposing a limiter defined in (4.50), based on positive cell averages. As shown in [31], such a limiter does not destroy the order of accuracy. Moreover, positivity of cell averages for each c_{ih} is achieved for $\beta_0>1$ and $\beta_1\in(1/8,1/4)$ when the coupling potential ψ is zero. For the general PNP system, we numerically identify parameter pairs (β_0,β_1) so that cell averages remain positive, as confirmed in Example 1.

In our numerical simulation with $k=1,2,3$, we use the second order explicit Runge–Kutta method (RK2, also called Heun's method) for time discretization to solve the ODE system of the form $\dot a=\mathfrak{L}(\mathbf{a},\mathbf{t})$:

$$\begin{aligned}\mathbf{a}^{(1)}&=\mathbf{a}^n+\Delta t\mathfrak{L}(\mathbf{a}^n,t_n),\\\mathbf{a}^*&=\mathbf{a}^{(1)}+\Delta t\mathfrak{L}(\mathbf{a}^1,t_{n+1}),\\\mathbf{a}^{n+1}&=\frac{1}{2}\mathbf{a}^n+\frac{1}{2}\mathbf{a}^*.\end{aligned}\tag{3.43}$$

Corollary 3.1. *Consider the RK2 time discretization (3.43). Assume that $c_{ih}^n(x)$ and the intermediate states $c_{ih}^{(1)}$ and c_{ih}^* are all positive in each I_j. There exists $\mu^*>0$ such that if the mesh ratio $\mu=\frac{\Delta t}{\Delta x^2}\in(0,\mu^*)$, then the fully discrete free energy*

$$F(c_h^n,\psi_h^n)=\sum_{j=1}^{N}\int_{I_j}\left[\sum_{i=1}^{m}c_{ih}^n\log c_{ih}^n+\frac{1}{2}\left(\sum_{i=1}^{m}q_ic_{ih}^n+\rho_0\right)\psi_h^n\right]dx+\frac{1}{2}\int_{\partial\Omega}\sigma\psi_h^nds$$

satisfies

$$F^{n+1}\le F^n,$$

provided that β_0 is suitably large, and $\beta_1=0$ in $Fl(\psi_h)$ defined in (2.13) and (2.16).

Proof. From (3.33) in Theorem 3.3 it follows that

$$F^* := F(c_h^*, \psi_h^*) \le F^{(1)} := F(c_h^{(1)}, \psi_h^{(1)}) \le F^n := F(c_h^n, \psi_h^n). \tag{3.44}$$

Note using (3.34c), F^n can also be written as

$$F^n = \sum_{j=1}^{N} \int_{I_j} \sum_{i=1}^{m} c_{ih}^n \log\left(c_{ih}^n\right) dx + \frac{1}{2} A_1\left(\psi_h^n, \psi_h^n\right).$$

Hence

$$F^{n+1} = \sum_{j=1}^{N} \int_{I_j} \left[\sum_{i=1}^{m} \left(\frac{1}{2} c_{ih}^n + \frac{1}{2} c_{ih}^* \right) \log\left(\frac{1}{2} c_{ih}^n + \frac{1}{2} c_{ih}^* \right) \right] dx + \frac{1}{2} A_1\left(\frac{1}{2}\psi_h^n + \frac{1}{2}\psi_h^*, \frac{1}{2}\psi_h^n + \frac{1}{2}\psi_h^* \right),$$

where by (3.43), we have used

$$c_{ih}^{n+1} = \frac{1}{2} c_{ih}^n + \frac{1}{2} c_{ih}^*; \quad \psi_h^{n+1} = \frac{1}{2}\psi_h^n + \frac{1}{2}\psi_h^*.$$

Using the fact that $A_1(w, w)$ is a convex functional in w in the sense that

$$A_1(\theta u + (1-\theta)v, \theta u + (1-\theta)v) \le \theta A_1(u, u) + (1-\theta) A_1(v, v), \forall \theta \in [0, 1],$$

which may be verified by the following identity

$$\theta A_1(u, u) + (1-\theta) A_1(v, v) - A_1(\theta u + (1-\theta)v, \theta u + (1-\theta)v) = \theta(1-\theta) A_1(u - v, u - v)$$

and $A_1(u - v, u - v) \ge 0$ from (3.22). Thus

$$A_1\left(\frac{1}{2}\psi_h^n + \frac{1}{2}\psi_h^*, \frac{1}{2}\psi_h^n + \frac{1}{2}\psi_h^* \right) \le \frac{1}{2} A_1(\psi_h^n, \psi_h^n) + \frac{1}{2} A_1(\psi_h^*, \psi_h^*). \tag{3.45}$$

Since $c \log c$ is convex in c, we also have

$$\left(\frac{1}{2} c_{ih}^n + \frac{1}{2} c_{ih}^* \right) \log\left(\frac{1}{2} c_{ih}^n + \frac{1}{2} c_{ih}^* \right) \le \frac{1}{2} c_{ih}^n \log\left(c_{ih}^n\right) + \frac{1}{2} c_{ih}^* \log\left(c_{ih}^*\right). \tag{3.46}$$

Equations (3.45) and (3.46) imply that

$$F^{n+1} \le \frac{1}{2} F^n + \frac{1}{2} F^*.$$

This together with (3.44) leads to $F^{n+1} \le F^n$, as claimed. □

Remark 3.5. Corollary 3.1 suggests that the DG scheme (2.12) with the time evolution by the strong stability preserving (SSP) Runge–Kutta method [49] does not increase the free energy at each time step, as long as the time step is suitably small. Hence high order SSP Runge–Kutta time discretization can be used for high order DG simulations, e.g., $k \ge 4$.

Remark 3.6. The time step restriction $\Delta t \sim O(\Delta x)^2$ is obviously a drawback of the explicit time discretization. Usually one would use implicit in time discretization for diffusion and explicit time discretization for the nonlinear drift term (called IMEX in the literature) so that the time step restriction could be relaxed. Unfortunately, formulation (2.11) does not support such a separation.

3.4. Preservation of steady states

If we start with initial data c_{ih}^0, already at steady states, i.e., $\log c_{ih}^0 + q_i \psi_h^0(x) = C_i$, it follows from (3.29b) that $p_{ih}^0 = C_i$. Furthermore, (3.29a) implies that $c_{ih}^1 = c_{ih}^0 \in V_h$, which when inserted into (3.29c) gives $\psi_h^1 = \psi_h^0$ (up to an constant, fixed to 0); hence $\log c_{ih}^1 + q_i \psi_h^1(x) = C_i$. By induction we have

$$\log c_{ih}^n + q_i \psi_h^n(x) = C_i, \quad \forall n \in \mathbb{N}.$$

This says that the DG scheme (3.29) preserves steady states. Moreover, we can show that in some cases the numerical solution tends asymptotically toward a steady state, independent of initial data. More precisely, we have the following result.

Theorem 3.4. *Let the assumptions in Theorem 3.3 be met, and $(c_{ih}^n, p_{ih}^n, \psi_h^n)$ be the numerical solution to the fully discrete DG scheme (3.29), then the limits of $(c_{ih}^n, p_{ih}^n, \psi_h^n)$ as $n \to \infty$ satisfy*

$$p_{ih}^* = C_i, \quad \log c_{ih}^n + q_i \psi_h^n(x) \in C_i + V_h^{\perp},$$

where C_i are some constants.

Proof. Since F^n is non-increasing and bounded from below, we have

$$\lim_{n\to\infty} F^n = \inf\{F^n\}.$$

Observe from (3.32) that

$$F^{n+1} - F^n \le -\frac{\Delta t}{2} \sum_{i=1}^{m} A_{c_{ih}^n}(p_{ih}^n, p_{ih}^n) \le 0.$$

When passing to the limit $n \to \infty$ we have $\lim_{n\to\infty} \sum_{i=1}^m A_{c_{ih}^n}(p_{ih}^n, p_{ih}^n) = 0$. This and the coercivity of $A_{c_{ih}^n}(p_{ih}^n, p_{ih}^n)$ imply the limit of p_{ih}^n, denoted by p_{ih}^*, must be constant in each computational cell and the whole domain. These when inserted into (3.29b) give the desired result. The proof is complete. □

4. Numerical implementation

4.1. Computing ψ_h

In order to compute a unique ψ_h, we fix $\psi(a)$ as being given, and define

$$Fl(\psi_h)(a) = \beta_0 \frac{(\psi_h^+ - \psi(a))}{h} + \frac{1}{2}(\sigma_a + \psi_{hx}^+), \quad \{\psi\} = (\psi_h^+ + \psi(a))/2, \tag{4.47a}$$

$$Fl(\psi_h)(b) = \sigma_b, \quad \{\psi\} = \psi_h^-. \tag{4.47b}$$

We add (2.12c) over all $j = 1 \cdots N$ and use the modified boundary condition (4.47) to obtain the following

$$A(\psi_h, v) = L(v), \quad \forall v \in V_h, \tag{4.48}$$

where

$$A(\psi_h, v) = A_1(\psi_h, v) + \left[\left(\beta_0 \frac{\psi_h^+}{h} + \frac{1}{2}\psi_{hx} \right) v^+ + \frac{1}{2}\psi_h^+ v_x^+ \right]_{x_{1/2}}$$

and

$$L(v) = \int_a^b \rho(x) v(x) dx + \left[\left(\beta_0 \frac{\psi(a)}{h} - \frac{1}{2}\sigma_a \right) v^+ + \frac{1}{2}\psi(a) v_x^+ \right]_{x_{1/2}} + \sigma_b v_{N+1/2}^-.$$

Lemma 4.1. *For $\beta_0 \ge \max\{\Gamma(\beta_1, 1), k^2\}$, and ρ given, there exists a unique ψ_h to (2.12c) with (2.13) and the boundary fluxes in (4.47).*

Proof. For the same reason as mentioned earlier, it suffices to prove the uniqueness. Let $v = \psi_{h1} - \psi_{h2}$ for two different solutions $\psi_{hi}, i = 1, 2$, then

$$A(v, v) = 0.$$

Note that

$$\begin{aligned} A(v, v) &= A_1(v, v) + \frac{\beta_0}{h}(v_{1/2}^+)^2 + (v v_x)_{1/2}^+ \\ &\ge \gamma \|v\|_E^2 + \frac{1}{2}\int_{I_1} v_x^2 dx + \frac{\beta_0}{2h}(v_{1/2}^+)^2 - \frac{h}{2\beta_0}(v_x^+)_{1/2}^2 \\ &\ge \gamma \|v\|_E^2 + \frac{\beta_0}{2h}(v_{1/2}^+)^2, \end{aligned} \tag{4.49}$$

provided that β_0 is large enough so that

$$\beta_0 \geq \sup_{v\in P^k(I_1)} \frac{h(v_x)_{1/2}^2}{\int_{I_1} v_x^2 dx} = \sup_{\eta\in P^{k-1}([-1,1])} \frac{2u^2(1)}{\int_{-1}^{1} u^2(\xi)d\xi} = \Gamma(0,1) = k^2.$$

Hence every term on the right of (4.49) must be zero, which yields $v \equiv 0$. Uniqueness thus follows. □

Remark 4.1. The above result provides a guide for the choices of (β_0, β_1) in numerically solving the Poisson equation. We shall take $\beta_1 = 0$ in solving the Poisson equation so that to also ensure the entropy dissipation property (see Theorem 3.2), hence it suffices to take $\beta_0 > k^2 = \Gamma(0,1)$.

4.2. Positivity-preserving limiter

In the scheme formulation involving the projection of $p_i = q_i\psi + logc_i$, concentrations c_{ih} need to be strictly positive at each time step, and we follow [31] to enforce positivity through some accuracy-preserving limiter based on positive cell averages.

Let $w_h \in P^k(I_j)$ be an approximation to a smooth function $w(x) \geq 0$, with cell averages $\bar{w}_j > \delta$ for δ being some small positive parameter or zero. We then consider another polynomial in $P^k(I_j)$ so that

$$w_h^\delta(x) = \bar{w}_j + \frac{\bar{w}_j - \delta}{\bar{w}_j - \min_{I_j} w_h(x)}(w_h(x) - \bar{w}_j), \quad \text{if } \min_{I_j} w_h(x) < \delta. \tag{4.50}$$

This reconstruction maintains same cell averages and satisfies

$$\min_{I_j} w^\delta(x) \geq \delta.$$

Lemma 4.2 *(cf. [31]). If $\bar{w}_j > \delta$, then w^δ satisfies the estimate*

$$|w^\delta(x) - w_h(x)| \leq C(k)\left(||w_h(x) - w(x)||_\infty + \delta\right), \quad \forall x \in I_j,$$

where $C(k)$ is a constant depending on k. This says that the reconstructed $w^\delta(x)$ in (4.50) does not destroy the accuracy when $\delta < h^{k+1}$.

4.3. Algorithm

The algorithm can be summarized in following steps.

1. (Initialization.) Project $c_i^{\text{in}}(x)$ onto V_h, as formulated in (2.14), to obtain $c_{ih}^0(x)$.
2. (Reconstruction.) From $c_{ih}^n(x)$, apply, if necessary, the reconstruction (4.50) to c_{ih}^n to ensure that in each cell $c_{ih}^n > \delta$.
3. (Poisson solver.) Solve (2.12c) to obtain ψ_h^n subject to the modified boundary fluxes (4.47).
4. (Projection.) Solve (2.12b) to obtain p_{ih}^n.
5. (Update.) Solve (2.12a) to update c_{ih}^{n+1} with some Runge–Kutta (RK) ODE solver.
6. Repeat steps 2–5 until final time T.

The implementation details are deferred to Appendix A.

5. Numerical examples

In this section, we present a selected set of examples in order to numerically validate our DDG scheme. In §5.1, we construct an example with exact solution known, and examine the order of accuracy by numerical convergence tests, while we quantify l_1 errors defined by

$$\|u_h - u_{ref}\|_{l_1} = \sum_{j=1}^{N} \int_{I_j} |u_h(x) - u_{ref}(x)|dx,$$

with the integral on I_j evaluated by a 4-point Gaussian quadrature method and u_{ref} being the exact solution. Long time simulation is also performed to illustrate how the positivity of cell averages propagates when using proper choices of (β_0, β_1). §5.2 is devoted to demonstrate the mass conservation, energy dissipation and preservation of the steady state. In §5.3 and §5.4, we apply the DDG scheme to a non-monovalent system and a reduced single species system.

Table 5.1
Error table of Example 1 at $T = 0.1$.

(k, β_0, β_1)	h	c_1 error	order	c_2 error	order	ψ error	order
$(1, 2, -)$	0.2	0.023279	–	0.031295	–	0.0033241	–
	0.1	0.0037603	2.5043	0.0059588	2.2582	0.0009351	1.8578
	0.05	0.00065589	2.4414	0.0012548	2.1909	0.0002603	1.8718
	0.025	0.00012745	2.3635	0.00028581	2.1343	6.9808e–05	1.8987
$(2, 4, 1/12)$	0.2	0.0028937	–	0.0030675	–	0.0012417	–
	0.1	0.00018926	3.6436	0.00024835	3.4352	0.00010034	3.4636
	0.05	1.391e–05	3.4981	2.2705e–05	3.3395	9.1444e–06	3.3808
	0.025	1.4824e–06	3.2301	2.4238e–06	3.2277	9.2476e–07	3.3057
$(3, 15, 1/4)$	0.2	0.0030963	–	0.0029231	–	0.0011002	–
	0.1	0.00023282	4.0764	0.00021924	3.9254	7.4195e–05	4.3897
	0.05	1.7512e–05	4.2480	1.6857e–05	4.0196	5.4161e–06	4.6393
	0.025	6.4483e–07	4.7633	8.3344e–07	4.3381	1.1946e–07	5.5027

5.1. Cell average and convergence test

In $\Omega = [0, 1]$, we consider

$$\begin{aligned}
\partial_t c_1 &= \partial_x(\partial_x c_1 + q_1 c_1 \partial_x \psi) + f_1,\\
\partial_t c_2 &= \partial_x(\partial_x c_2 + q_2 c_2 \partial_x \psi) + f_2,\\
-\partial_x^2 \psi &= q_1 c_1 + q_2 c_2,\\
\partial_x \psi(t, 0) = 0, &\quad \partial_x \psi(t, 1) = -e^{-t}/60,\\
\partial_x c_i + q_i c_i \partial_x \psi &= 0, \quad x = 0, 1,
\end{aligned}$$

with

$$\begin{aligned}
f_1 &= \frac{(50x^9 - 198x^8 + 292x^7 - 189x^6 + 45x^5)}{30e^{2t}} + \frac{(-x^4 + 2x^3 - 13x^2 + 12x - 2)}{e^t},\\
f_2 &= \frac{(x-1)(110x^9 - 430x^8 + 623x^7 - 393x^6 + 90x^5)}{60e^{2t}} + \frac{(x-1)(x^4 - 2x^3 + 21x^2 - 16x + 2)}{e^t}.
\end{aligned}$$

This system, with $q_1 = 1$ and $q_2 = -1$, admits exact solutions

$$\begin{aligned}
c_1 &= x^2(1-x)^2 e^{-t},\\
c_2 &= x^2(1-x)^3 e^{-t},\\
\psi &= -(10x^7 - 28x^6 + 21x^5)e^{-t}/420.
\end{aligned}$$

We also set $\psi(t, 0) = 0$ to pick out a particular solution since ψ is unique up to an additive constant. This extra condition is numerically enforced according to (4.47).

We first test positivity of cell averages for P^2 polynomials with $(\beta_0, \beta_1) = (4, 1/12)$ in (2.13) for p_{ih}. Note that the reconstruction is necessary in this example since $c_i = 0 < \delta$ at $x = 0, 1$. Our simulation with the reconstruction (4.50) up to $T = 100$ indicates that the cell averages remain positive.

Table 5.1 displays both l_1 errors and orders of convergence when using P^k elements at $T = 0.1$. We observe that order of convergence is roughly of $k+1$. Fig. 5.1 shows the numerical solution at different times. In the top of Fig. 5.1, we observe that the numerical solutions (dots) match the exact solutions (solid line) at $t = 1$ very well. At $t = 5$, our numerical approximation still captures the solution profile very well when the magnitude of the concentrations is close to zero ($\sim 10^{-4}$). In the presence of the source terms f_1 and f_2, one should not expect to have either mass conservation or free energy decay.

5.2. Mass conservation and free energy dissipation

We consider the following problem on the domain $[0, 1]$,

$$\begin{aligned}
\partial_t c_i &= \partial_x(\partial_x c_i + q_i c_i \partial_x \psi), \quad i = 1, 2,\\
-\partial_x^2 \psi &= q_1 c_1 + q_2 c_2,\\
\partial_x \psi = 0, &\quad \partial_x c_i = 0, \quad i = 1, 2, \quad x = 0, 1,
\end{aligned}$$

where q_1 and q_2 are set to be 1 and -1, respectively, with initial conditions

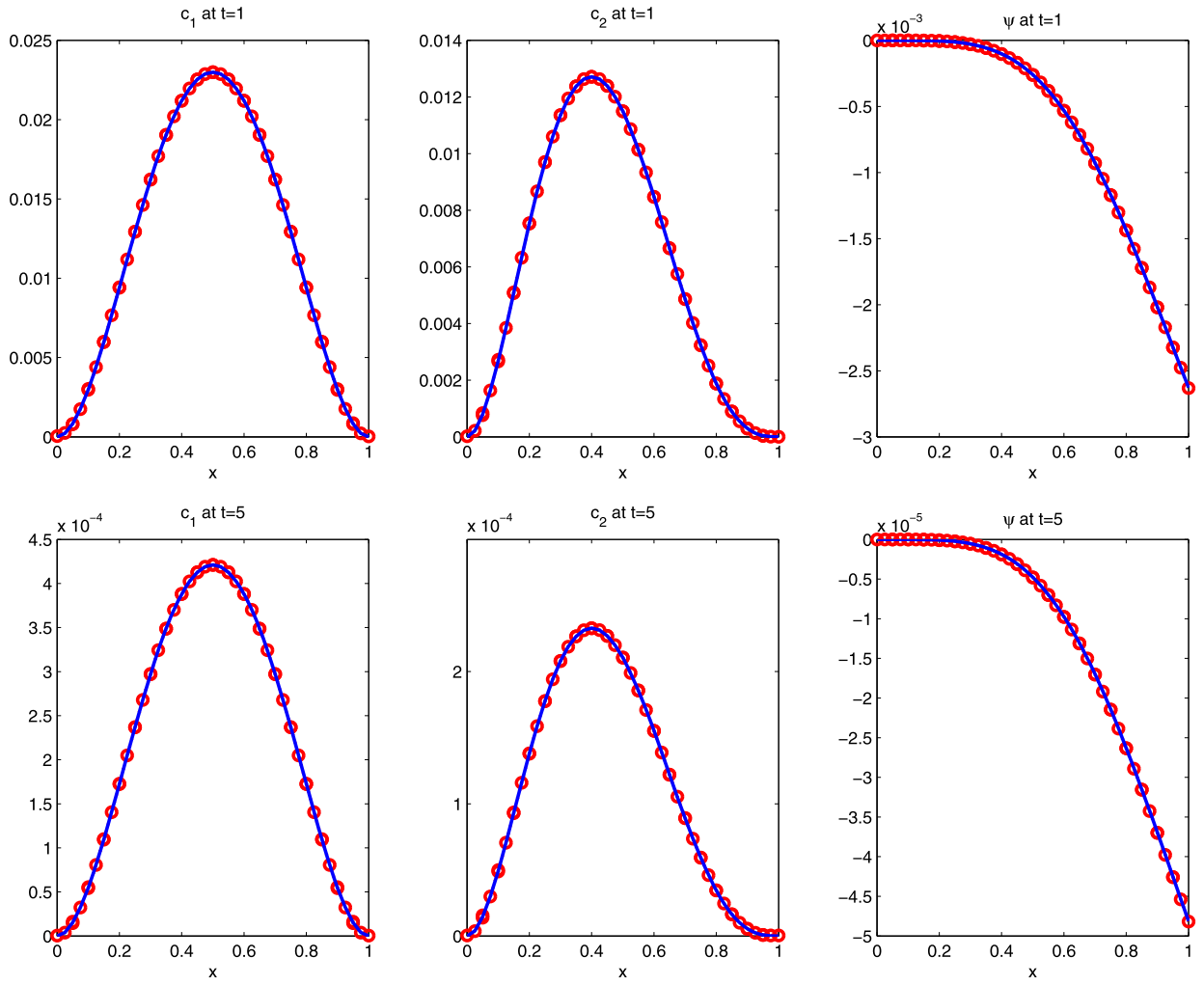

Fig. 5.1. Numerical solution (dots) versus exact solution (solid line) at $t = 1$ and $t = 5$.

$$c_1^{\text{in}}(x) = 1 + \pi \sin(\pi x), \quad c_2^{\text{in}}(x) = 4 - 2x,$$

which satisfies the compatibility condition (1.2).

With zero flux for concentration c_1 and c_2, this model example is to test the conservation of total mass and free energy decay. In Fig. 5.2 (top), we see the snapshots of c_1, c_2 and ψ at $t = 0, 0.01, 0.1, 0.8, 1$. We observe that the solutions at $t = 0.8$ and $t = 1$ are indistinguishable. Obviously the solution is converging to the steady state, which has constant $c_1 = 3$, $c_2 = 3$ and $\psi = 0$. Fig. 5.2 (bottom) shows the energy decay (see the change on the right vertical axis) and conservation of mass (see the left vertical axis). We see that the total mass of c_1 and c_2 stays constant all the time while the free energy is decreasing monotonically. In fact the free energy levels off after $t = 0.2$, at which the system is already in steady state.

5.3. Non-monovalent system and nonzero fixed charge

We consider the following non-monovalent system (monovalent if $q_1 = -q_2 = 1$) with nonzero fixed charge ρ_0 in $[0, 1]$.

$$\begin{aligned}
\partial_t c_1 &= \partial_x(\partial_x c_1 + q_1 c_1 \psi_x),\\
\partial_t c_2 &= \partial_x(\partial_x c_2 + q_2 c_2 \psi_x),\\
-\partial_x^2 \psi &= q_1 c_1 + q_2 c_2 + \rho_0,
\end{aligned}$$

with $q_1 = 1$, $q_2 = -2$ and $\rho_0 = 12(x - 0.5)^2$. The initial and boundary conditions are

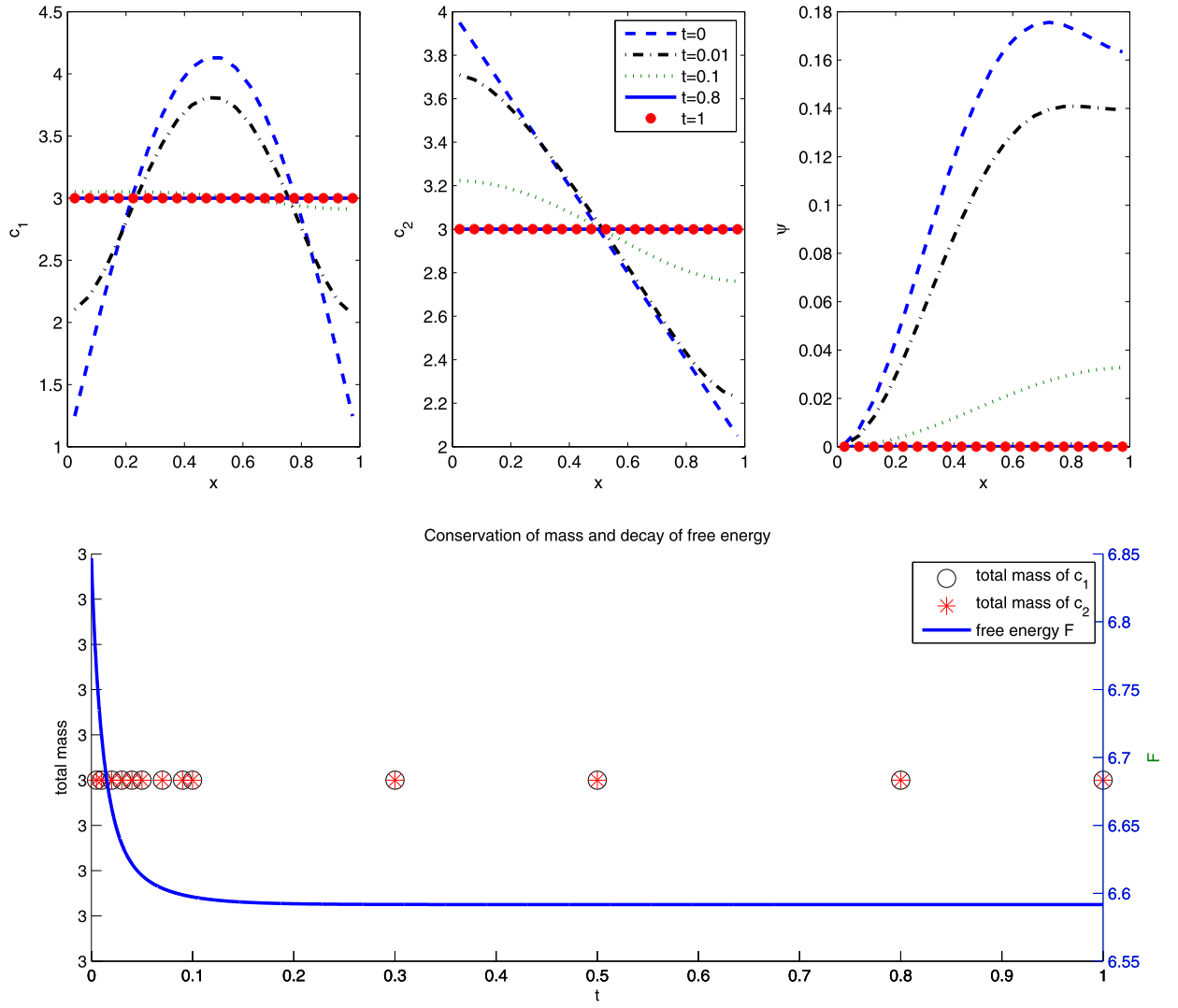

Fig. 5.2. Temporal evolution of the solutions.

$$c_1^{\text{in}}(x) = 2 + 12(x-0.5)^2, \quad c_2^{\text{in}}(x) = 1 + 2x,$$
$$\partial_x c_i + q_i c_i \partial_x \psi = 0, \quad x = 0, 1,$$
$$\partial_x \psi(t,0) = \partial_x \psi(t,1) = 0,$$

where the compatibility condition (1.2) is satisfied since $\int_0^1 (q_1 c_1^{\text{in}} + q_2 c_2^{\text{in}} + \rho_0) dx = 0$.

In Fig. 5.3 (top) are the snapshots of c_1, c_2 and ψ at $t = 0, 0.01, 0.1, 0.8, 1$. Fig. 5.3 (bottom) shows the energy decay (see the change on the right vertical axis) and conservation of mass (see the left vertical axis). The concentrations c_1 and c_2 have different total mass but both are conserved in time. We observe that the system is at steady states after $t = 0.2$, which are no longer constants due to the nonzero fixed charge ρ_0.

5.4. Single species

Finally we consider the reduced model (1.6) of single species. The problem is

$$\partial_t c = \partial_x(\partial_x c + c\partial_x \psi), \quad x \in [0,1],\ t > 0,$$
$$-\partial_x^2 \psi = c, \quad x \in [0,1],$$

subject to initial and boundary conditions

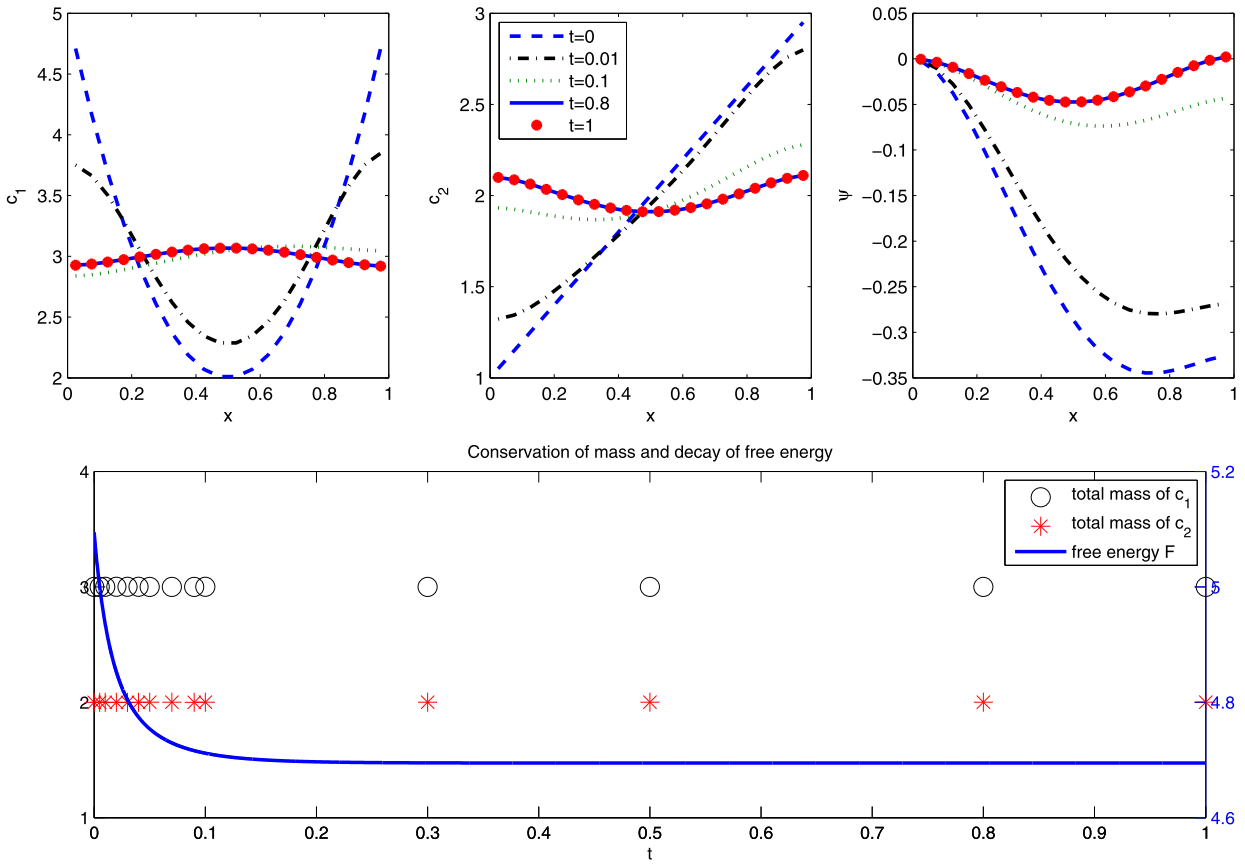

Fig. 5.3. Non-monovalent system and nonzero fixed charge.

$$c(0,x)=2-x;\quad \partial_x\psi(t,0)=0;\quad \partial_x\psi(t,1)=-3/2;\quad \partial_x c+c\partial_x\psi=0,\quad x=0,1,$$

which satisfies the compatibility condition (1.2).

Fig. 5.4 displays the dynamic behavior of c (top left) and of ψ (top right), as well as the mass conservation and energy decay (bottom). Note that the steady state of the concentration c is not a constant in this case due to the nonzero boundary flux $\partial_x\psi(t,1)$, i.e., ions are attracted to the boundary $x=1$.

6. Concluding remarks

In this paper, we developed an arbitrary high order DG method to solve initial boundary value problems for the Poisson–Nernst–Planck system, which is a mean field type model for concentrations of chemical species. The semi-discrete DG method has been shown to conserve the mass and satisfy the corresponding discrete free energy dissipation law. The fully discrete DG method with the Euler forward time discretization also satisfies the free energy dissipation law under a restriction on the time step relative to the square of the spatial mesh size. Moreover, the free energy does not increase at each time step for the RK2 method (3.43) as well as for the strong stability preserving (SSP) Runge–Kutta method of any high order. The method also preserves the steady states. These nice properties are also confirmed by our numerical tests. For proper choices of numerical flux parameters (β_0,β_1) in our numerical experiments, we find that each cell average remains positive if it is initially positive. This is needed to update numerical solutions at each time step so they are positive. In future work we will apply our method to multi-dimensional problems and explore more efficient ways to preserve positivity of numerical solutions.

Acknowledgments

This work was supported by the National Science Foundation under Grant DMS1312636 and by NSF Grant RNMS (Ki-Net) 1107291.

Appendix A

In this appendix, we give details related to the implementation of the method.

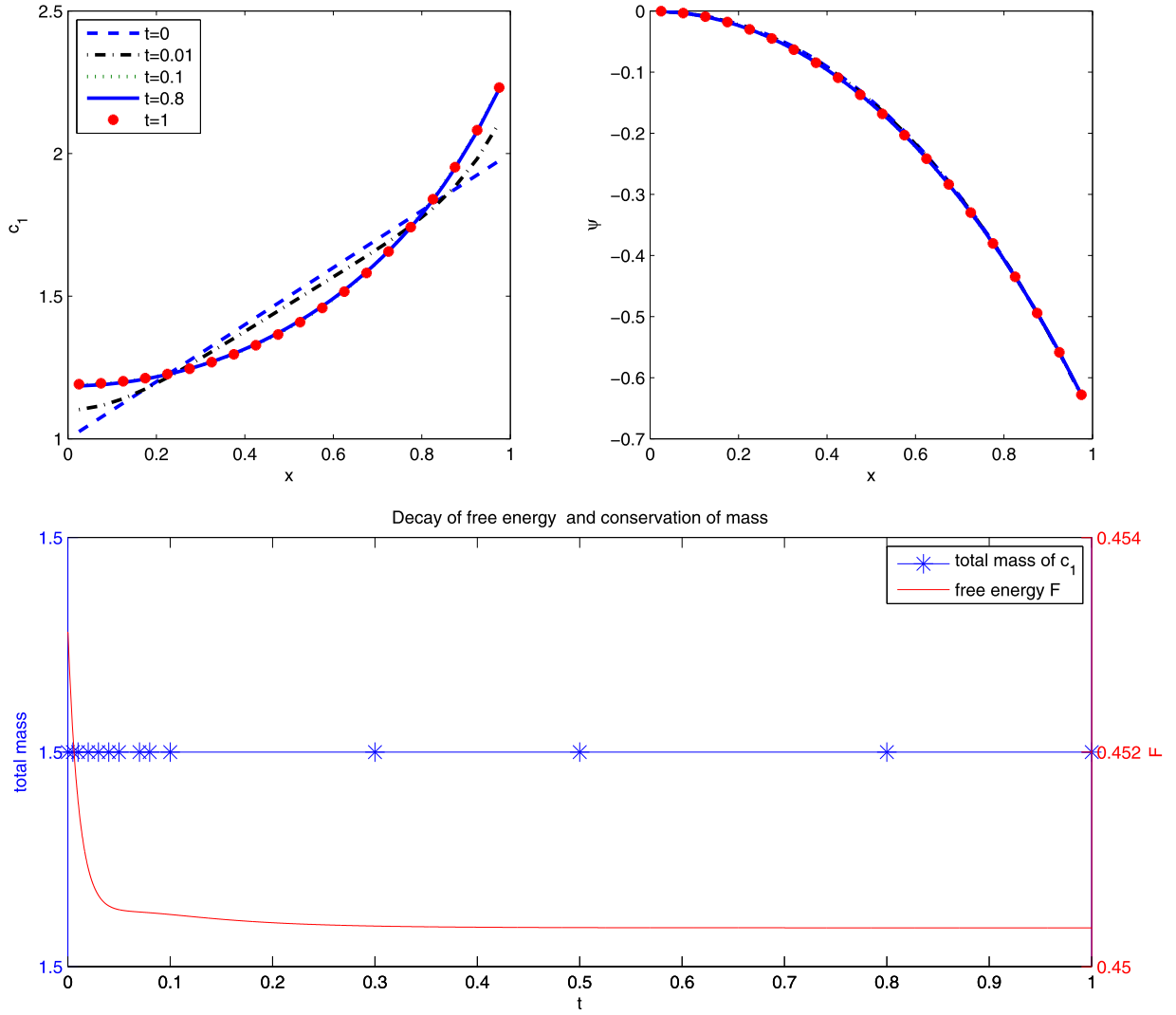

Fig. 5.4. Single species.

The kth order basis functions in a 1-D standard reference element $\xi \in [-1, 1]$ are taken as the Legendre polynomials $\{L_l(\xi)\}_{l=0}^{k}$. The numerical solutions $c_{ij}(t, x)$, $p_{ij}(t, x)$ and $\psi_i(t, x)$ in each cell I_j, after dropping subscript h for convenience, can be expressed as

$$c_{ij}(t,x) = \sum_{l=0}^{k} c_{ij}^{l}(t) L_l(\xi) = L^{\top}(\xi) c_{ij}(t),$$

$$\psi_j(t,x) = \sum_{l=0}^{k} \psi_j^{l}(t) L_l(\xi) = L^{\top}(\xi) \psi_j(t),$$

$$p_{ij}(t,x) = \sum_{l=0}^{k} p_{ij}^{l}(t) L_l(\xi) = L^{\top}(\xi) p_{ij}(t),$$

using the map $x = x_j + \frac{h}{2}\xi$, with notation $L^{\top} = (L_0, L_1, \cdots, L_k)$ and $c_{ij} = (c_{ij}^0, \cdots, c_{ij}^k)^{\top}$. With such an expression, the numerical fluxes at $x_{j+1/2}$ become

$$h\widehat{\partial_x p_i} = \beta_0 (L^{\top}(-1) p_{i,j+1} - L^{\top}(1) p_{ij}) + (L_{\xi}^{\top}(-1) p_{i,j+1} + L_{\xi}^{\top}(1) p_{ij}) + 4\beta_1 (L_{\xi\xi}^{\top}(-1) p_{i,j+1} - L_{\xi\xi}^{\top}(1) p_{ij}),$$

$$h\widehat{\partial_x\psi} = \beta_0(L^\top(-1)\psi_{j+1} - L^\top(1)\psi_j) + L_\xi^\top(-1)\psi_{j+1} + L_\xi^\top(1)\psi_j,$$
$$\widehat{\psi} = \frac{1}{2}(L^\top(1)\psi_j + L^\top(-1)\psi_{j+1}).$$

This when substituted into (2.12c) gives

$$A\psi_{j-1} + B\psi_j + C\psi_{j+1} = hK\sum_{i=1}^{m} q_i c_{ij} + \frac{h^2}{2}\sum_{n=1}^{Q_1}\omega_n\rho_0(x_j + hs_n/2)L(s_n), \quad 2 \le j \le N-1, \tag{A-1}$$

where

$$A = -L(-1)(\beta_0 L(1) - L_\xi(1))^\top - L_\xi(-1)L^\top(1),$$
$$B = 2\int_{-1}^{1} L_\xi L_\xi^\top d\xi + L(-1)(\beta_0 L(-1) + L_\xi(-1))^\top + L(1)(\beta_0 L(1) - L_\xi(1))^\top$$
$$+ L_\xi(-1)L^\top(-1) - L_\xi(1)L^\top(1),$$
$$C = -L(1)(\beta_0 L(-1) + L_\xi(-1))^\top + L_\xi(1)L^\top(-1),$$
$$K = \frac{h}{2}\int_{-1}^{1} L(\xi)L^\top(\xi)d\xi.$$

Here Q_1-point Gauss quadrature rule on the interval $(-1,1)$ is used to integrate $\rho_0(x_j + h\xi/2)L(\xi)$. We choose $Q_1 \ge \frac{k+2}{2}$ points so that the quadrature rule has accuracy of at least $O(h^{k+2})$ order. Boundary conditions are specified in section 2.2. Note that the resulting $(k+1)N \times (k+1)N$ matrix is a sparse block matrix, which can be inverted efficiently.

We then compute (2.12b) by the same quadrature rule

$$Kp_{ij} = q_i K\psi_j + \frac{h}{2}\sum_{n=1}^{Q_1}\omega_n log(L^\top(s_n)c_{ij})L(s_n). \tag{A-2}$$

Finally we simplify (2.12a) to get the following ODE system

$$K\dot{c}_{ij} = \frac{2}{h}R_1 + \frac{1}{2h}(R_2 + R_3), \quad 2 \le j \le N-1, \tag{A-3}$$

where

$$R_1 = -\sum_{n=1}^{Q_2}\omega_n L^\top(s_n)c_{ij}L_\xi^\top(s_n)p_{ij}L_\xi(s_n),$$
$$R_2 = (L^\top(1)c_{ij} + L^\top(-1)c_{i,j+1})(-D^\top p_{ij} + E^\top p_{i,j+1})L(1)$$
$$- (L^\top(1)c_{i,j-1} + L^\top(-1)c_{ij})(-D^\top p_{i,j-1} + E^\top p_{ij})L(-1) = R_2^+ - R_2^-,$$
$$R_3 = (L^\top(1)c_{ij} + L^\top(-1)c_{i,j+1})(L^\top(1)p_{ij} - L^\top(-1)p_{i,j+1})L_\xi(1)$$
$$+ (L^\top(1)c_{i,j-1} + L^\top(-1)c_{ij})(L^\top(1)p_{i,j-1} - L^\top(-1)p_{ij})L_\xi(-1) =: R_3^+ + R_3^-.$$

Here

$$D = \beta_0 L(1) - L_\xi(1) + 4\beta_1 L_{\xi\xi}(1), \quad E = \beta_0 L(-1) + L_\xi(-1) + 4\beta_1 L_{\xi\xi}(-1).$$

In the evaluation of R_1, we choose $Q_2 \ge \frac{k+4}{2}$ points. In implementation, since $Q_2 > Q_1$, we simply use Q_2 Gaussian quadrature points in integrating both ρ_0 and $\log(c_i)$.

At two end cells, R_1 is still valid. The zero flux conditions (1.1d) are used to obtain R_2 and R_3, i.e., at $j = 1$, we use $R_2 = R_2^+$, $R_3 = R_3^+$, and at $j = N$ we use $R_2 = -R_2^-$, $R_3 = -R_3^-$. The discrete ODE system is then solved by the RK2 method (3.43).

References

[1] A. Arnold, P. Markowich, G. Toscani, On large time asymptotics for drift–diffusion–Poisson systems, Transp. Theory Stat. Phys. 29 (3–5) (2000) 571–581.
[2] A.M. Anile, N. Nikiforakis, V. Romano, G. Russo, Discretization of semiconductor device problems. II, Handb. Numer. Anal. XIII (2005) 443–522.
[3] M.Z. Bazant, K.T. Chu, B.J. Bayly, Current–voltage relations for electrochemical thin films, SIAM J. Appl. Math. 65 (2005) 1463.
[4] M. Burger, V. Capasso, D. Morale, On an aggregation model with long and short range interactions, Nonlinear Anal., Real World Appl. 8 (2007) 939–958.

[5] A. Blanchet, J.A. Carrillo, P. Laurencot, Critical mass for a Patlak–Keller–Segel model with degenerate diffusion in higher dimensions, Calc. Var. Partial Differ. Equ. 35 (2) (2009) 133–168.
[6] P. Biler, J. Dolbeault, Long time behavior of solutions to Nernst–Planck and Debye–Hückel drift–diffusion systems, Ann. Henri Poincaré 1 (3) (2000) 461–472.
[7] M. Burger, M.D. Francesco, Large time behavior of nonlocal aggregation models with nonlinear diffusion, Netw. Heterog. Media 3 (4) (2008) 749–785.
[8] P. Biler, W. Hebisch, T. Nadzieja, The Debye system: existence and large time behavior of solutions, Nonlinear Anal. 23 (1994) 1189–1209.
[9] F. Brezzi, L. Marini, S. Micheletti, P. Pietra, R. Sacco, S. Wang, Discretization of semiconductor device problems. I, Handb. Numer. Anal. 13 (2005) 317–441.
[10] J. Bedrossian, N. Rodríguez, A.L. Bertozzi, Local and global well-posedness for aggregation equations and Patlak–Keller–Segel models with degenerate diffusion, Nonlinearity 24 (2011) 168–714.
[11] D.S. Bolintineanu, A. Sayyed-Ahmad, H.T. Davis, Y.N. Kaznessis, Poisson–Nernst–Planck models of nonequilibrium ion electrodiffusion through a protegrin transmembrane pore, PLoS Comput. Biol. 5 (1) (2009) e1000277.
[12] H. Cohen, J. Cooley, The numerical solution of the time-dependent Nernst–Planck equations, Biophys. J. 5 (1965) 145–162.
[13] A.E. Cardenas, R.D. Coalson, M.G. Kurnikova, Three-dimensional Poisson–Nernst–Planck theory studies: influence of membrane electrostatics on gramicidin A channel conductance, Biophys. J. 79 (1) (2000) 80–93.
[14] C. Chainais-Hillairet, F. Filbet, Asymptotic behavior of a finite volume scheme for the transient drift–diffusion model, IMA J. Numer. Anal. 27 (4) (2007) 689–716.
[15] C. Chainais-Hillairet, J.G. Liu, Y.J. Peng, Finite volume scheme for multi-dimensional drift–diffusion equations and convergence analysis, M2AN Math. Model. Numer. Anal. 37 (2) (2003) 319–338.
[16] J.H. Chaudhry, J. Comer, A. Aksimentiev, L. Olson, A stabilized finite element method for modified Poisson–Nernst–Planck equations to determine ion flow through a nanopore, Commun. Comput. Phys. 15 (1) (2014).
[17] S. Datta, Electronic Transport in Mesoscopic Systems, Cambridge University Press, 1997.
[18] B. Eisenberg, W. Liu, Poisson–Nernst–Planck systems for ion channels with permanent charges, SIAM J. Math. Anal. 38 (2007) 1932–1966.
[19] W. Fang, K. Ito, Global solutions of the time-dependent drift–diffusion semiconductor equations, J. Differ. Equ. 123 (1995) 523–566.
[20] W. Fang, K. Ito, Asymptotic behavior of the drift–diffusion semiconductor equations, J. Differ. Equ. 123 (1995) 567–587.
[21] H. Gajewski, K. Gröger, On the basic equations for carrier transport in semiconductors, J. Math. Anal. Appl. 113 (1986) 12–35.
[22] H. Gajewski, K. Gärtner, On the discretization of Van Roosbroeck's equations with magnetic field, Z. Angew. Math. Mech. 76 (5) (1996) 247–264.
[23] S. Glasstone, An Introduction to Electrochemistry, D. Van Nostrand Company, Inc., Princeton, NJ, 1942.
[24] J.S. Hesthaven, T. Warburton, Nodal Discontinuous Galerkin Methods: Algorithms, Analysis, and Applications, Springer, New York, 2007.
[25] B. Hille, Ion Channels and Excitable Membranes, 3rd ed., Sinauer Associates, Inc., Sunderland, MA, 2001.
[26] J.W. Jerome, Analysis of Charge Transport: A Mathematical Study of Semiconductor Devices, Springer, Berlin, 1996.
[27] M.G. Kurnikova, R.D. Coalson, P. Graf, A. Nitzan, A lattice relaxation algorithm for three-dimensional Poisson–Nernst–Planck theory with application to ion transport through the gramicidin A channel, Biophys. J. 76 (1999) 642–656.
[28] D. Li, Electrokinetics in Microfluidics, vol. 2, Academic Press, 2004.
[29] H. Liu, Optimal error estimates of the direct discontinuous Galerkin method for convection–diffusion equations, Math. Comput. 84 (295) (2015) 2263–2295.
[30] H. Liu, Z. Wang, A free energy satisfying finite difference method for Poisson–Nernst–Planck equations, J. Comput. Phys. 268 (2014) 363–376.
[31] H. Liu, Z. Wang, An entropy satisfying discontinuous Galerkin method for nonlinear Fokker–Planck equations, J. Sci. Comput. 68 (3) (2016) 1217–1240.
[32] H. Liu, J. Yan, The direct discontinuous Galerkin (DDG) methods for diffusion problems, SIAM J. Numer. Anal. 47 (2009) 675–698.
[33] H. Liu, J. Yan, The direct discontinuous Galerkin (DDG) method for diffusion with interface corrections, Commun. Comput. Phys. 8 (3) (2010) 541–564.
[34] H. Liu, H. Yu, An entropy satisfying conservative method for the Fokker–Planck equation of the finitely extensible nonlinear elastic dumbbell model, SIAM J. Numer. Anal. 50 (2012) 1207–1239.
[35] H. Liu, H. Yu, The entropy satisfying discontinuous Galerkin method for Fokker–Planck equations, J. Sci. Comput. 62 (2015) 803–830.
[36] H. Liu, H. Yu, Maximum-principle-satisfying third order discontinuous Galerkin schemes for Fokker–Planck equations, SIAM J. Sci. Comput. 36 (5) (2014) A2296–A2325.
[37] B. Lu, Y.C. Zhou, G.A. Huber, S.D. Bond, M.J. Holst, J.A. McCammon, Electrodiffusion: a continuum modeling framework for biomolecular systems with realistic spatiotemporal resolution, J. Chem. Phys. 127 (2007) 135102.
[38] B.Z. Lu, M.J. Holst, J.A. McCammon, Y.C. Zhou, Poisson–Nernst–Planck equations for simulating biomolecular diffusion–reaction processes I: finite element solutions, J. Comput. Phys. 229 (19) (2010) 6979–6994.
[39] P.A. Markowitch, The Stationary Semiconductor Device Equations, Springer, Wien, 1986.
[40] M.S. Mock, Analysis of Mathematical Models of Semiconductor Devices, vol. 3, Boole Press, 1983.
[41] M. Mirzadeha, F. Giboua, A conservative discretization of the Poisson–Nernst–Planck equations on adaptive Cartesian grids, J. Comput. Phys. 274 (2014) 633–653.
[42] P.A. Markowich, C.A. Ringhofer, C. Schmeiser, Semiconductor Equations, Springer-Verlag Inc., New York, 1990.
[43] M.S. Metti, J. Xu, C. Liu, Energetically stable discretizations for charge transport and electrokinetic models, J. Comput. Phys. 306 (2016) 1–18.
[44] W. Nernst, Die elektromotorische wirksamkeit der ionen, Z. Phys. Chem. 4 (1889).
[45] M. Planck, Über die erregung von electricitąt und wärme in electrolyten, Annu. Phys. Chem. 39 (1880).
[46] A. Prohl, M. Schmuck, Convergent discretizations for the Nernst–Planck–Poisson system, Numer. Math. 111 (2009) 591–630.
[47] B. Rivière, Discontinuous Galerkin Methods for Solving Elliptic and Parabolic Equations: Theory and Implementation, SIAM, Philadelphia, 2008.
[48] C.-W. Shu, Discontinuous Galerkin methods: general approach and stability, in: Numerical Solutions of Partial Differential Equations, in: Adv. Courses Math. CRM Barcelona, Birkhäuser, Basel, 2009, pp. 149–201.
[49] C.-W. Shu, S. Osher, Efficient implementation of essentially non-oscillatory shock-capturing schemes, J. Comput. Phys. 77 (1988) 439–471.
[50] T. Sokalski, A. Lewenstam, Application of Nernst–Planck and Poisson equations for interpretation of liquid-junction and membrane potentials in real-time and space domains, Electrochem. Commun. 3 (3) (2001) 107–112.
[51] T. Sokalski, P. Lingenfelter, A. Lewenstam, Numerical solution of the coupled Nernst–Planck and Poisson equations for liquid junction and ion selective membrane potentials, J. Phys. Chem. B 107 (11) (2003) 2443–2452.
[52] C.M. Topaz, A.L. Bertozzi, M.A. Lewis, A nonlocal continuum model for biological aggregation, Bull. Math. Biol. 68 (2006) 1601–1623.
[53] G.W. Wei, Q. Zheng, Z. Chen, K. Xia, Variational multiscale models for charge transport, SIAM Rev. 54 (2012) 699–754.
[54] Q. Zheng, D. Chen, G.-W. Wei, Second-order Poisson–Nernst–Planck solver for ion channel transport, J. Comput. Phys. 230 (13) (2011) 5239–5262.